RESEARCH   **Open Access**

A Hysteretic Constitutive Model for Reinforced Concrete Panel Elements

Kutay Orakcal[1*] , Leonardo M. Massone[2] and Denizhan Ulugtekin[1]

Abstract

A simple yet effective constitutive model-referred to as the "Fixed Strut Angle Model" (FSAM)-is presented in this paper for simulating the nonlinear axial/shear behavior of reinforced concrete membrane (panel) elements subjected to generalized and reversed cyclic loading conditions. In the formulation of the FSAM, normal stresses in cracked concrete are calculated along fixed crack (strut) directions. Shear stresses developing along crack surfaces, which are calculated using a simple friction-based constitutive relationship, are superimposed with the concrete stresses along the struts, for obtaining the total stress field in concrete. Model predictions were compared with panel tests results available in the literature, at various global and local response levels. The model was demonstrated to reasonably capture the overall response characteristics of reinforced concrete panels, including hysteretic shear stress vs. strain behavior, shear stress capacity, hysteretic shear stiffness attributes, ductility, pinching behavior, governing failure mode, principal strain and stress directions, and local deformations.

Keywords: panel, membrane, hysteretic, constitutive, model, concrete, crack, shear, wall

1 Introduction

With adaptation of performance-based seismic design and assessment methodologies for reinforced concrete (RC) structures, analytical modeling of the behavior of RC members under generalized loading conditions induced by earthquake actions has recently gained substantial importance among engineers and researchers. A reliable prediction of the nonlinear earthquake response of structural systems inherently requires the use of analytical models that can accurately capture the hysteretic behavior of individual structural members, as well as their interaction within a structural system.

In seismic design of RC buildings, use of structural walls is effective for resisting earthquake actions. To counteract earthquake demands in the nonlinear response range, slender walls are designed and detailed to yield in flexure, and to undergo inelastic flexural deformations without loss of lateral load capacity. Therefore, a modeling methodology that appropriately accounts for

nonlinear flexural behavior becomes sufficient for design and evaluation purposes. However, shear-controlled squat walls (with aspect ratios typically less than 1.5) are also common in low-rise construction and at lower levels of tall buildings (for example, parking-level walls or basement walls), as well as in perimeter walls with perforations due to window and door openings. For low aspect-ratio walls or wall segments, behavior is often dominated by nonlinear shear responses, and the modeling parameters selected for shear stiffness and strength can have a significant impact on the predicted distribution of member forces and on building lateral drift. As well, obtaining reliable predictions for local deformations (e.g., amplified compressive strains at wall boundary regions associated with plane sections not remaining plane due to shear deformations) and capturing of nonlinear shear and shear-flexure interaction responses (as well as a realistic value for the effective shear stiffness) in also slender and medium-rise walls are still topics of utmost interest. For performance-based design and evaluation of RC systems with structural walls, there is still a need for simple yet robust modeling approaches that capture coupled axial, shear, and flexural responses of walls with various aspect ratios and response characteristics.

---

*Correspondence: kutay.orakcal@boun.edu.tr
[1] Dept. of Civil Engineering, Bogazici University, 34342 Bebek, Istanbul, Turkey
Full list of author information is available at the end of the article

Simulation of the nonlinear response of walls can be accomplished by using finite element (microscopic) or phenomenological (macroscopic) modeling approaches. For use in finite element models, various constitutive model formulations for monotonic (e.g., Modified Compression Field Theory (Vecchio and Collins 1986), Rotating-Angle Softened Truss Model (Pang and Hsu 1995), Fixed-Angle Softened Truss Model (Pang and Hsu 1996), Disturbed Stress Field Model (Vecchio 2000), Softened Membrane Model (Hsu and Zhu 2002)) and cyclic (e.g., Ohmori et al. 1989; Stevens et al. 1991; Vecchio 1999; Palermo and Vecchio 2003; Mansour and Hsu 2005; Gérin and Adebar 2009) loading have been proposed for simulating the nonlinear response of RC panels. However, most of these models are not implemented in commonly-used open-source computational platforms for analysis of structural walls or wall systems. Although not open-source, finite element analysis software incorporating hysteretic formulations of the Modified Compression Field Theory (Vecchio and Collins 1986) and the Disturbed Stress Field Model (Vecchio 2000) is available online (http://vectoranalysisgroup.com). The Cyclic Softened Membrane Model (Mansour and Hsu 2005) has been implemented in the open-source platform Open-Sees (http://opensees.berkeley.edu); however, studies on simulating the nonlinear response of structural walls using the Cyclic Softened Membrane Model are limited. It is believed that there is still a need for development, experimental validation, and open-source implementation of simple yet sufficiently accurate constitutive models to be used for nonlinear response analysis of structural walls or structural systems incorporating walls.

Therefore, an original constitutive model formulation has been developed by the authors for simulating the hysteretic response of RC panel (membrane) elements under generalized in-plane loading conditions. The model formulation is based on interpretation and simplification of previous modeling approaches. The constitutive model was implemented (Kolozvari et al. 2015a, 2018c) in the open-source computational platform OpenSees (http://opensees.berkeley.edu) as a plane-stress constitutive relationship for reinforced concrete panel elements. As well, the FSAM has already been used as a constitutive model element in both macroscopic (fiber-based) (Kolozvari et al. 2015b, c, 2018a, 2019b) and finite element (Gullu et al. 2018, 2019; Gullu and Orakcal 2019) model formulations developed for RC walls, and has been shown to provide accurate response predictions for walls with various aspect ratios and response characteristics. This paper provides a detailed description of the mechanical constitution of the FSAM, and provides results of detailed correlation studies conducted between FSAM predictions and RC panel test results obtained from two different experimental programs reported in the literature, for experimental validation of its fundamental working principles at the stress–strain level.

2 Model Background and Description

During the past three decades, significant efforts on understanding and simulating the inelastic shear behavior of RC members have focused on developing constitutive models capable of predicting the in-plane behavior of RC panel elements subjected to membrane actions. The pioneering modeling approaches, known as the first rotating-angle approaches (Vecchio and Collins 1986; Pang and Hsu 1995), were developed for monotonic loading conditions, and they simulated RC panel response using uniaxial constitutive relationships for concrete in tension and compression applied along the principal strain directions of the panel, together with uniaxial constitutive laws for reinforcing steel bars applied along rebar directions, with perfect bond assumed between concrete and reinforcing steel. This modeling approach treated cracked concrete as a new material and incorporated the smeared-crack approach, which considers average stresses and strains in concrete throughout the panel element, for satisfying the equilibrium conditions. Although the simplicity of the rotating-angle approach lies in the assumption that the principal stress direction in concrete coincides with the principal strain direction, interpretation of the rotating-angle modeling approach on how damage progresses in a RC panel element might be ambiguous, since once a crack develops at a particular location on a RC panel or wall, the crack direction remains the same and the crack progressively opens, closes, and re-opens with successive load cycles. Other modeling approaches for RC panels have also been proposed, based on either a fixed crack angle that follows the principal direction of the applied stresses (Pang and Hsu 1996; Hsu and Zhu 2002; Mansour and Hsu 2005), or an angle "lag" that deviates the principal strain and stress directions (Vecchio 2000; Stevens et al. 1991). The fixed-crack-angle approach used in the original Fixed-Angle Softened Truss Model (Pang and Hsu 1996) or its subsequent versions (Hsu and Zhu 2002; Mansour and Hsu 2005) is different from the approach used in this study in the sense that it assumes that the fixed crack directions coincide with the principal directions of the "applied" stress field on the panel element (necessitating proportional loading conditions applied on the RC panel), whereas the present model formulation does not require proportional loading.

Various cyclic constitutive panel models (Ohmori et al. 1989; Stevens et al. 1991; Vecchio 1999; Palermo and Vecchio 2003; Mansour and Hsu 2005; Gérin and Adebar 2009), incorporating rotating- or fixed-angle approaches,

Orakcal *et al. Int J Concr Struct Mater*   (2019) 13:51

Page 3 of 23

have also been developed based on results of cyclic test programs conducted on RC panel specimens (Ohmori et al. 1989; Stevens 1987; Mansour 2001). Test observations reported in the literature indicate that after formation of cracks in a RC panel, the direction of the principal stresses in concrete does not change significantly with loading, whereas the principal strain direction in the panel may undergo significant variation (Stevens et al. 1991). The principal stress directions in concrete being insensitive to loading implies that after formation of cracks, the principal stress directions in concrete follow approximately the fixed crack directions. This observation contradicts the assumption that the principal strain and concrete principal stress directions coincide, and also implies that shear stresses along the crack have marginal influence on the concrete principal stress directions. To consider this phenomenon in various formulations of the Disturbed Stress Field Model (Vecchio 2000; Stevens et al. 1991), which uses a rotating-crack assumption, an "angle lag" is empirically defined for the purpose of deviating the principal strain and stress directions in concrete. On the other hand, the Cyclic Softened Membrane Model (Mansour and Hsu 2005), although follows a fixed-crack-angle formulation, retains the assumption that the principal strain and stress directions in concrete coincide under cyclic loading.

A more simplistic approach is used in this study. The constitutive model described herein, which is named the "Fixed-Strut-Angle Model" (FSAM), incorporates a rotating-angle approach only until the first crack forms on the RC panel, the direction of which coincides with the direction of the principal strains applied on the panel element direction at the instant of cracking. Upon formation of the crack, the "baseline" formulation of the model (which neglects the shear stress along the crack surface) converts into a fixed-angle approach that inherently fixes the angle of the crack as the principal stress direction in concrete, meaning that stresses in concrete consist of normal stresses calculated parallel and perpendicular to the crack direction. As assumed by most other RC panel models available in the literature, identical strain fields are assumed to act on concrete and reinforcing steel components of a RC panel, based on the perfect bond assumption between concrete and reinforcing steel bars. It is also assumed that reinforcing bars develop zero shear stresses perpendicular to their longitudinal direction, which implies no dowel action on reinforcement. As well, behavioral features of concrete associated with the Poisson's ratio are neglected in the model formulation, for simplicity. While only uniaxial stresses develop in the longitudinal direction of reinforcing bars, the behavior of concrete is characterized by stress–strain relationships applied along biaxial directions, the orientation of

which are fixed after cracking. On top of this baseline formulation of the FSAM, where the shear stress transfer mechanism across cracks is neglected, a simple and friction-based constitutive relationship is adopted, and the shear aggregate interlock stresses developing along crack surfaces are superimposed with the concrete stresses developing along the crack directions. This superposition creates a marginal deviation between the crack directions and the new principal stress directions in concrete, and provides a reasonably accurate prediction of the overall behavior of the panel element, as shown later in this paper. Working principles of the FSAM are described in the following sections.

2.1 Uncracked Panel Response

The stress vs. strain behavior of uncracked concrete is simulated using a rotating-strut (rotating-crack) approach [similarly to the "Modified Compression Field Theory" (Vecchio and Collins 1986) and the "Rotating-Angle Softened Truss Model" (Pang and Hsu 1995)]. The strain field applied on concrete is transformed into principal strain directions and a uniaxial stress–strain relationship for concrete is applied along the principal strain directions, for obtaining the principal stresses in concrete. The principal strain directions imposed on the panel element are therefore assumed to coincide the with principal stress directions in concrete. A monotonic stress–strain relationship is adopted for concrete in the uncracked state, since the monotonic and hysteretic stress–strain behavior of concrete in a panel element subjected hysteretic loading can be assumed to not differ significantly prior to first cracking. This assumption was also made to overcome the difficulties to track and store history variables in the hysteretic stress–strain relationship for concrete, along rotating stress and strain directions in a panel.

For a given (applied) strain field (ε_x, ε_y, γ_{xy}), the principal strains (ε_1, ε_2) and the principal strain direction (θ) for the uncracked panel (Fig. 1a) are calculated. The principal stresses in concrete are then obtained using the principal strain values and the monotonic envelope of the constitutive material model for concrete. Uniaxial stresses in the reinforcing steel bars (σ_{sx}, σ_{sy}) developing under normal strains are determined based on the monotonic envelope of the uniaxial constitutive material model for reinforcing steel in each of the two orthogonal (x and y) directions of reinforcement, and are smeared over the panel based on the reinforcement ratios (ρ_{sx}, ρ_{sy}). The equilibrium of the panel model after including concrete and steel components (σ_x, σ_y, τ_{xy}), in Cartesian coordinates, becomes:

$$\sigma_x = \frac{\sigma_{c1} + \sigma_{c2}}{2} + \frac{\sigma_{c1} - \sigma_{c2}}{2} \cdot cos2\theta + \rho_{sx} \cdot \sigma_{sx} \quad (1)$$
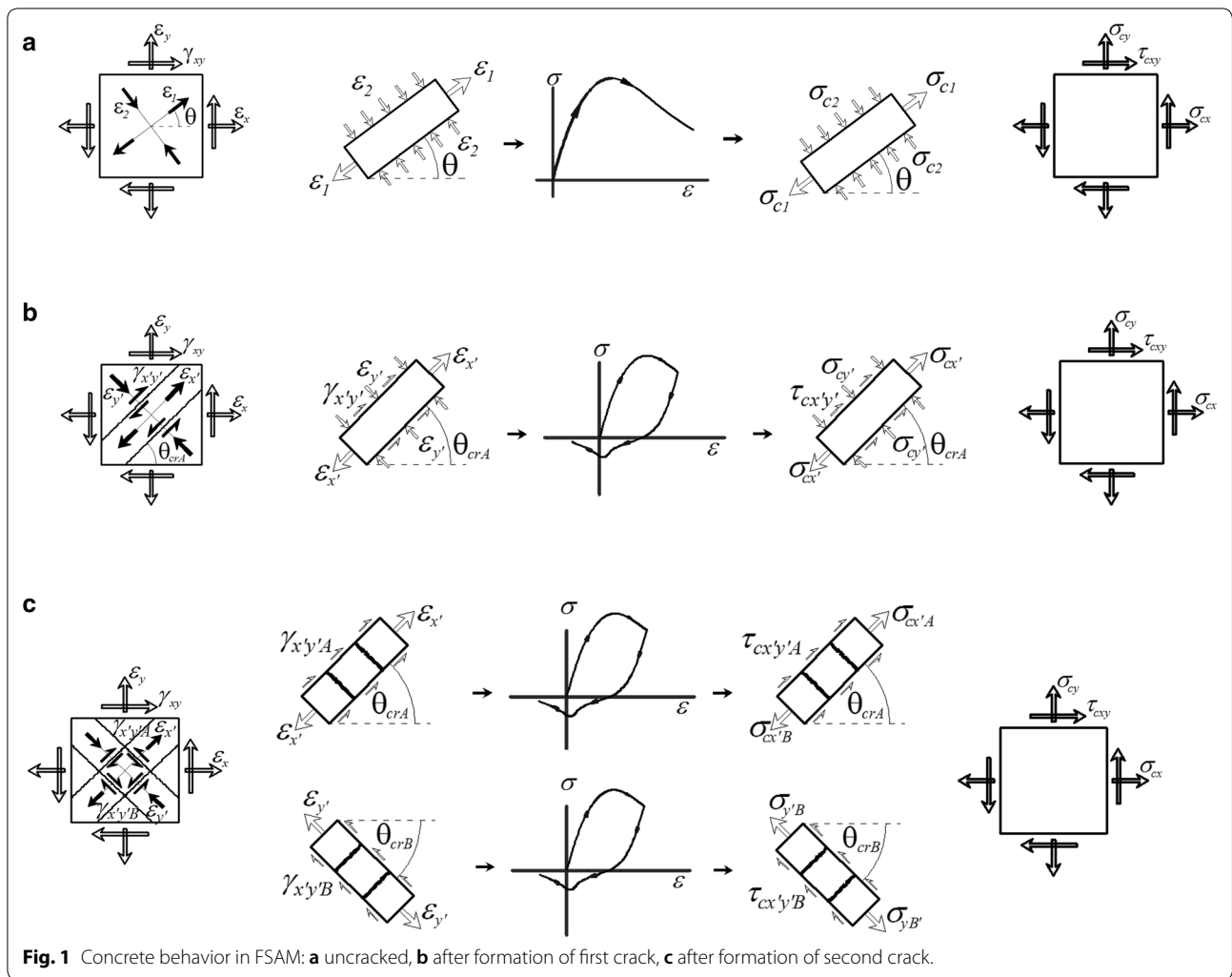
Fig. 1 Concrete behavior in FSAM: **a** uncracked, **b** after formation of first crack, **c** after formation of second crack.

$$\sigma_y = \frac{\sigma_{c1} + \sigma_{c2}}{2} - \frac{\sigma_{c1} - \sigma_{c2}}{2} \cdot cos2\theta + \rho_{sy} \cdot \sigma_{sy} \quad (2)$$

$$\tau_{xy} = \frac{\sigma_{c1} - \sigma_{c2}}{2} \cdot sin2\theta \quad (3)$$

2.2 Panel Response after Formation of First Crack

At the instant when the principal tensile strain in concrete first exceeds the concrete cracking strain (ε_t), the first crack develops, and the principal strain direction corresponding to first cracking is assigned as the first "fixed strut" (first crack) direction in the panel (θ_{crA}). After the first crack forms, while principal strain directions continue to rotate based on the strain field applied, the directions of the principal stresses in concrete are assumed to be fixed, as parallel and perpendicular to the

first fixed strut direction. This implies that the first crack (or strut) direction coincides with the principal stress directions in concrete, under the condition that zero shear stress develops along the crack.

The concrete uniaxial strains ($\varepsilon_{x'}$, $\varepsilon_{y'}$) in the direction of the first crack become (Fig. 1b):

$$\varepsilon_{x'} = \frac{\varepsilon_x + \varepsilon_y}{2} + \frac{\varepsilon_x - \varepsilon_y}{2} \cdot cos2\theta_{crA} + \frac{\gamma_{xy}}{2} \cdot sin2\theta_{crA} \quad (4)$$

$$\varepsilon_{y'} = \frac{\varepsilon_x + \varepsilon_y}{2} - \frac{\varepsilon_x - \varepsilon_y}{2} \cdot cos2\theta_{crA} - \frac{\gamma_{xy}}{2} \cdot sin2\theta_{crA} \quad (5)$$

Since the first strut direction is fixed (θ_{crA}), a uniaxial and hysteretic stress–strain relation for concrete (Fig. 1b) can be applied in directions parallel and perpendicular to the first strut (in order to obtain $\sigma_{cx'}$ and $\sigma_{cy'}$), and history variables in the constitutive

Orakcal *et al. Int J Concr Struct Mater*   (2019) 13:51

Page 5 of 23

stress–strain model for concrete can easily be tracked and stored along the two fixed directions. It should be mentioned that although the stress–strain relationship used for concrete is fundamentally uniaxial in nature, it also incorporates biaxial softening effects including compression softening and hysteretic biaxial damage. The equilibrium equations in x–y coordinates including the reinforcing steel component therefore become:

$$\sigma_x = \frac{\sigma_{cx'} + \sigma_{cy'}}{2} + \frac{\sigma_{cx'} - \sigma_{cy'}}{2} \cdot cos2\theta_{crA} + \rho_{sx} \cdot \sigma_{sx}$$
(6)

$$\sigma_y = \frac{\sigma_{cx'} + \sigma_{cy'}}{2} - \frac{\sigma_{cx'} - \sigma_{cy'}}{2} \cdot cos2\theta_{crA} + \rho_{sy} \cdot \sigma_{sy}$$
(7)

$$\tau_{xy} = \frac{\sigma_{cx'} - \sigma_{cy'}}{2} \cdot sin2\theta_{crA}$$
(8)

The analysis continues following a single fixed-strut mechanism until the second crack forms, at which stage the second strut is activated in the panel model. During the first strut stage, the model tracks the concrete stress vs. strain behavior along the first strut direction, and when the normal strain along the first strut first exceeds the "cyclic" cracking strain ($\varepsilon_{c0} + \varepsilon_t$ in Fig. 2a—also depends on the plastic strain upon reversal from a compressive stress), the second crack develops. Not considering the shear (aggregate interlock) stress developing on the crack surface allows the simplification that the second crack will form in perpendicular direction to the first crack, according to a principal-stress-based cracking criterion, Although various other cracking criteria may be utilized for definition of the second crack direction (e.g., relating the formation or direction of
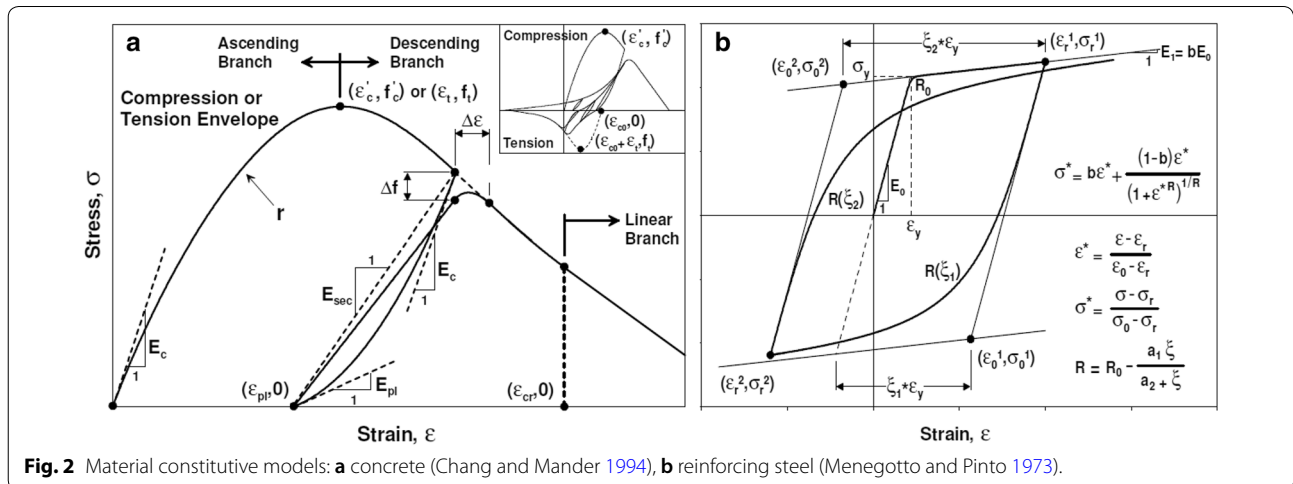
the second crack with principal strains), this approach was selected for its simplicity.

2.3 Panel Response After Formation of Second Crack
At the instant of the second crack formation, the second "fixed strut" will develop in parallel direction to the second crack (in perpendicular direction to the first strut). During further loading, the concrete stress field comprises two independent struts, working under interchanging compression and tension (Fig. 1c), based on the applied strain field. While the principal direction of the applied strain field continues to rotate during subsequent loading, the principal stress directions in concrete are assumed to be fixed along the two strut directions, again when zero shear stresses (zero shear aggregate interlock) are assumed to develop along the two crack surfaces. Since both strut directions are fixed, the hysteretic uniaxial stress vs. strain relationship adopted for concrete can be applied along the first and second strut directions. Using the uniaxial constitutive material model for concrete, the unsoftened principal stresses in concrete are first calculated, leading to the softened principal stresses ($\sigma_{cx'}$ and $\sigma_{cy'}$) after applying the softening due to history damage of concrete in compression and actual tensile strain in the orthogonal direction of each compression strut. For calculation of concrete stresses along the struts, the applied strain field should be transformed into normal strains parallel to the first and the second strut directions, instead of principal strain directions.

2.4 Shear Stress Transfer Across Cracks
As described above, the baseline formulation of the FSAM considers that when shear stresses transferred across cracks are neglected (i.e., when the crack surfaces are assumed frictionless), the concrete principal stress

Fig. 2 Material constitutive models: **a** concrete (Chang and Mander 1994), **b** reinforcing steel (Menegotto and Pinto 1973).

directions and crack directions coincide. However, this baseline formulation allows the flexibility to separately implement a constitutive relationship in the FSAM for representing shear stress transfer across cracks (e.g., a shear stress vs. shear strain relationship along a crack), since the model formulation allows calculating shear strains along the cracks. In RC members, sliding along cracks is known to develop shear aggregate interlock action, resulting in shear stress along crack surfaces. The zero-aggregate-interlock assumption incorporated in the baseline formulation of the FSAM may result in overestimation of sliding deformations along cracks, depending on the loading conditions (stress state) applied on the panel element.

Therefore, on top of the baseline formulation of the FSAM described above, a simple friction-based constitutive relationship for shear aggregate interlock is implemented, which relates the maximum shear stress developing along a crack surface to the compressive stress in concrete in perpendicular direction to the crack through a friction coefficient (Fig. 3). The adopted interlock model starts with linear loading/unloading behavior that relates the sliding shear (shear slip) strain along a crack to the shear stress developing on the crack surface, using a simple linear elastic relationship. However, the shear stress is reduced to zero when the normal stress in concrete in perpendicular direction to the crack is tensile (crack open); and is bounded by the product of a friction coefficient (η) and the normal stress in concrete perpendicular to the crack ($\sigma_{\perp c}$), when the concrete normal stress is compressive (crack closed). The slope of the linear elastic region of the shear stress vs. sliding strain relationship can be taken as a large value, where a value of $G = 0.4E_c$ was adopted in the present formulation of FSAM. Previous experimental and analytical studies on sliding shear behavior along concrete cracks [e.g., Tassios and Vintzeleou 1987] have shown that in the hysteretic shear stress vs. crack slip behavior, the slope of the transition from shear stresses in one direction to the other (upon reversal of slip deformation) can be idealized as infinitely large, irrespective of the magnitude of the compressive stress perpendicular to the crack surface. However, in the mathematical formulation of the FSAM, a finite slope is necessary to define the transition, for numerical stability of the model. It was observed in the model results that as long as a sufficiently large stiffness (such as E_c or $G = 0.4E_c$) is defined for the transition region, the hysteretic shear stress vs. slip behavior along the crack surface almost never falls on that transition, which makes the FSAM results insensitive to the magnitude of that slope. What controls the model response is the shear stress magnitude along the plastic region of the shear friction behavior, which is related to the varying compressive stress in concrete perpendicular to the crack surface, through the friction coefficient. Based on comparison of model predictions with test results obtained from the two experimental programs considered in this paper, an optimal friction coefficient value of $\eta = 0.1$ was selected for the tests by Stevens (1987), and $\eta = 0.2$ for the tests by Mansour (2001), as discussed in the relevant sections of this paper. Under constant compressive stress in concrete perpendicular to the crack, this model yields an elasto–plastic shear aggregate interlock behavior under cyclic loading, similar to the cyclic stress–strain behavior of reinforcing steel with no strain hardening. It must be mentioned that although much more refined constitutive models for shear aggregate interlock (that also considers crack width, crack spacing, the so-called "clamping" effect of reinforcing bars, etc.), or other empirical relationships representing shear stress transfer across cracks can be implemented in the formulation of the FSAM, this friction-based model was selected for its simplicity, and also because it is more suitable for smooth crack surfaces (Tassios and Vintzēleou 1987). Uniformly-oriented cracks with relatively smooth surfaces were assumed to develop in the panel specimens investigated, since they were subjected to uniform stress distributions. The present FSAM formulation also assumes that no shear stress is resisted by the reinforcing steel bars in their transverse direction, implying no dowel action on the reinforcement. However, the model also provides the flexibility to implement dowel action into its formulation.
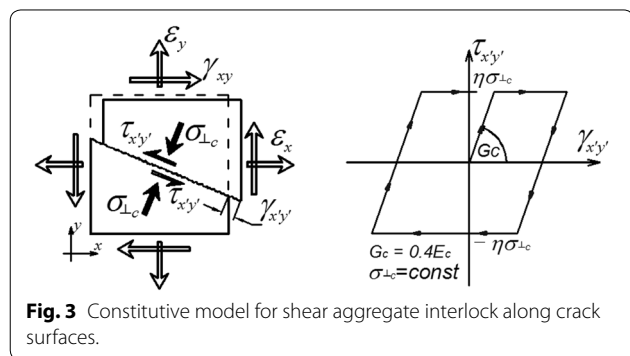
2.5 Material Constitutive Models

2.5.1 Concrete

The hysteretic uniaxial constitutive model by Chang and Mander (1994) was implemented in the formulation of the FSAM for representing the stress vs. strain behavior of concrete. The Chang and Mander (1994) model is a refined non-dimensional model that can reproduce the generalized hysteretic behavior of ordinary or high-strength, confined or unconfined concrete

Fig. 3 Constitutive model for shear aggregate interlock along crack surfaces.

Orakcal *et al. Int J Concr Struct Mater*   (2019) 13:51

Page 7 of 23

under continuous reversed cyclic compression and tension. The model formulation reflects important behavioral characteristics such as the hysteretic transition from compression to tension and vice versa, the progressive degradation of stiffness of the unloading and reloading curves for increasing values of strain, and the effects of and gradual crack closure and tension stiffening on the behavior.

In the Chang and Mander (1994) model, the monotonic curve forms the envelope for the hysteretic stress–strain relationship. Concrete in tension is modeled with a cyclic behavior similar to that in compression. The model envelopes for compression and tension can be calibrated for the slope of the stress vs. strain relationship at the origin, and the shape of both the pre-peak and post-peak branches of the stress–strain behavior. The shape of the envelopes can be feasibly altered while keeping the values of the peak stress and the strain at peak stress constant. In order to define the compression and tension envelopes, Chang and Mander (1994) model uses the Tsai's equation (1988), which is based on the equation by Popovics (1973), an equation that has proven to be very useful in describing the monotonic compressive stress–strain curve for concrete. In order to define the cyclic properties of concrete in compression, statistical regression analyses were performed by Chang and Mander (1994) on an extensive experimental database. Based on the regression analyses, empirical relations were developed for key hysteretic parameters such as those for secant stiffness and plastic stiffness upon unloading from the envelope, and stress and strain offsets upon return to the compression envelope (Fig. 2a). Further details of the model can be found in the report by Chang and Mander (1994).

2.5.2 Reinforcing Steel

The uniaxial constitutive stress–strain relationship implemented in the FSAM for reinforcing steel is the well-known nonlinear hysteretic model of Menegotto and Pinto (1973), extended by Filippou et al. (1983) for incorporating isotropic strain hardening effects, as a relatively simple yet effective model that can accurately simulate the hysteretic stress–strain behavior of reinforcing steel bars.

In the Menegotto and Pinto model, the stress–strain (σ–ε) relationship is in the form of curved transitions (Fig. 2b), each from a straight-line asymptote with slope E_0 (modulus of elasticity) to another straight-line asymptote with slope $E_1 = b \cdot E_0$ (yield modulus) where the parameter b is the strain hardening ratio. The curvature of the transition curve between the two asymptotes is governed by a cyclic curvature parameter (R), which permits the Bauschinger's effect to be represented. It must

be emphasized that more robust stress–strain models for reinforcing steel, which also incorporate more sophisticated behavioral characteristics relevant to the seismic behavior and performance of reinforced concrete structures, including local or global inelastic bar buckling [e.g., (Massone and Moroder 2009; Massone and López 2014)], low-cycle fatigue degradation, and corrosion effects [e.g., (Tripathi et al. 2018; Kashani et al. 2015)], can easily be implemented in the FSAM formulation. The simple stress–strain model adopted in this study does not incorporate such features, since the panel test programs used for validating the working principles of the FSAM did not present any of these particular failure or degradation mechanisms.

2.5.3 Compression Softening in Concrete

An important consideration in modeling the behavior of a RC panel element under membrane actions is incorporating the compression softening effect. The softening effect for the behavior of concrete under biaxial stress state has been experimentally observed by many researchers, [e.g., Vecchio and Collins (1986)], and has been represented by analytical models mainly in the form of reduction (softening) in the compressive stresses in concrete along the principal compression direction of RC panels, due to presence of tensile strains in the perpendicular principal direction. Some compression softening models have also included softening in the compressive strain [e.g., Belarbi and Hsu (1995); Vecchio and Collins (1993)], reducing the strain at the peak compressive stress for concrete. Although all of these compression softening models were formulated for the case of monotonic loading, many of them were implemented into cyclic analysis methods (Belarbi and Hsu 1995; Vecchio and Collins 1993).

In this study, the so-called "Model B" by Vecchio and Collins (1993), which considers only a reduction in the peak compressive stress, was implemented in the FSAM, due to its suitability for implementation into a hysteretic panel model formulation. In this approach, only the compressive stresses in concrete along the principal compression direction are reduced by the β_m coefficient, whereas the strain at the peak compressive stress on the monotonic stress vs. strain envelope of concrete is assumed not to be influenced by the tensile strain in the perpendicular direction. The softening coefficient β_m is defined as:

$$\beta_m = \frac{1}{1 + 0.27 \cdot \left(\frac{\varepsilon_1}{\varepsilon_0} - 0.37 \right)} \tag{9}$$

where ε_1 is the tensile strain in the principal tensile stress direction and ε_0 is the strain corresponding to peak stress of concrete in compression.

Orakcal *et al. Int J Concr Struct Mater*   (2019) 13:51

Page 8 of 23

2.5.4 Tension Stiffening Effect on Concrete and Steel

The contribution of cracked concrete to the tensile resistance of RC members is known as the effect of tension stiffening. The concrete between the cracks, which is still bonded to the reinforcing steel bars, contributes to the tensile resistance of the member. The tension stiffening phenomenon plays a significant role in reducing the post-cracking deformations of reinforced concrete structures, and has been proven by researchers (Pang and Hsu 1995; Stevens 1987; Belarbi and Hsu 1994; Bentz 2005; Mansour et al. 2002) to influence considerably the post-cracking stiffness, yield capacity and shear behavior of reinforced concrete members.

In formulation of the FSAM, two alternative tension stiffening models available in the literature were incorporated. The first tension stiffening model used is the model by Belarbi and Hsu (1994) [used for comparison of model results with tests by Mansour (2001)]. As investigated in detail by Belarbi and Hsu (1994), modeling of the tension stiffening phenomenon must consider two effects simultaneously. First, an average (smeared) tensile stress–strain curve must be considered for cracked concrete; and second, the stress–strain curve of bare mild steel bars must be replaced by an average (smeared) stress–strain curve for steel bars stiffened by concrete between cracks. In the Belarbi and Hsu (1994) model, the tensile stress–strain (σ_c, ε_c) behavior of concrete is considered as linear up to cracking (f_{cr}, ε_{cr}) and, a descending curve is defined for the post-cracked stress–strain region as $\sigma_c = f_{cr}(\varepsilon_{cr}/\varepsilon_c)^{0.4}$. Belarbi and Hsu also identified how the average stress–strain relationship of reinforcing steel bars surrounded by concrete is different than the stress–strain relationship of bare steel bars. The most important difference was found to be the lowering of the yield stress, as yielding of a reinforced concrete element occurs when the steel stress at the cracked section reaches the yield strength of the bare bar. At the same time, the average steel stress smeared along the length of the element reaches a level lower than that of the yield stress of the bare bar. Based on experimental data from the RC panels, the effective (reduced) yield stress for embedded reinforcing bars is expressed, in terms of the elastic modulus ratio n (E_s/E_c), the reinforcement ratio ρ, concrete cracking stress f_{cr}, and bare bar yield stress f_y, as:

$$f_{y\,eff} = f_y \cdot \left[1 - 1.314 \cdot \frac{n^{0.434}}{\rho^{1.084}} \cdot \left(\frac{f_{cr}}{f_y} \right)^{1.517} \right]. \quad (10)$$

The second tension stiffening model incorporated in the FSAM is the model by Stevens (1987) (used for comparison of model results with tests by Stevens (1987)). In the Stevens (1987) model, average tensile stress–strain behavior of concrete is also considered as linear up to

cracking, after which an exponential curve is defined as $f_c = f_{cr} \cdot \left[(1 - \alpha) \cdot e^{-\lambda_t \cdot (\varepsilon_c - \varepsilon_{cr})} + \alpha \right]$, with a so-called homogeneity ratio called ($\alpha = 75 \cdot \rho / d_b$, $\lambda_t = 270/\sqrt{\alpha}$). The effective yield stress of reinforcing steel bars is defined by Stevens to be dependent on bar diameter (d_b) and concrete cracking stress (f_{cr}) as:

$$f_{y\,eff} = f_y - 75/d_b \cdot f_{cr} \quad (11)$$

The reason that two different constitutive models for tension stiffening were used in the FSAM formulation for comparison of model results with test results is that the tension stiffening model is not a unique attribute of the FSAM. The researchers (Mansour 2001; Stevens 1987) who conducted the panel tests considered in this study for experimental validation of the FSAM have stated that the two tension stiffening models (Belarbi and Hsu 1994; Stevens 1987) best represent the experimentally-observed behavior of their test specimens. Therefore, the FSAM was experimentally-validated for the two respective test programs, with the two respective tension stiffening models in its formulation, for a more consistent evaluation of its performance. As discussed in detail by Bentz (2005), the difference between these two tension stiffening models can be attributed to differences in the reinforcement configuration of the panel specimens tested by Stevens (1987) and Mansour (2001) with regards to the bond characteristics of the reinforcing steel bars, which are influenced by bar diameter and spacing.

2.5.5 Biaxial Damage on Concrete

An important consideration in modeling the behavior of a RC panel element under membrane actions is incorporating the cyclic damage effects on concrete subjected to biaxial loading. This cyclic damage on concrete is represented via a damage coefficient. Unlike compression softening and tension stiffening parameters, the damage coefficient is a cyclic-strain-history-dependent parameter, and is not considered in analysis of concrete under monotonic loading.

The damage coefficient is a parameter that considers the effect of the history of compressive strains, which are in perpendicular direction to a specific compressive stress direction considered (e.g., along a compression strut) for concrete. The damage coefficient is therefore defined for biaxial loading, and does not apply for uniaxial concrete stress–strain behavior. The damage coefficient, similar to the compression softening coefficient, is applied as a multiplier to the concrete compressive stress, softening the stress–strain behavior of concrete in compression.

Similarly to the approach used for incorporating tension stiffening in the FSAM, two alternative empirical models available in literature for the damage coefficient

were implemented in the formulation of the FSAM for the experimental validation studies presented in this paper; one by Stevens (1987) (used for comparison of model results with tests by Stevens (1987)), and the other by Mansour et al. (2002) [used for comparison of model results with tests by Mansour (2001)]. The formulation proposed by Stevens (1987) uses the ratio of the difference between the maximum value of the compressive strain experienced ($\varepsilon_{\perp \max}$) and the current compressive strain ($\varepsilon_\perp$) (if any) in the direction perpendicular to the compressive (strut) direction considered, to the peak compressive stress, (ε'_c) in concrete, as:

$$\beta_{damage} = 1 \Big/ \left(1 + 0.5 \cdot (\varepsilon_{\perp \max} - \varepsilon_\perp) \Big/ \varepsilon'_c \right) \qquad (12)$$

On the other hand, the biaxial damage formulation proposed by Mansour et al. (2002) uses the ratio of the maximum value of the compressive strain experienced in the direction perpendicular to the compressive (strut) direction considered, to the peak compressive stress, (ε'_c) in concrete, as:

$$\beta_{damage} = (1 - 0.4 \cdot \varepsilon_{\perp \max} \Big/ \varepsilon'_c) \qquad (13)$$

The final softening parameter used in this study considering both compression softening and biaxial damage parameters takes the form of $\beta = \beta_m \cdot \beta_{damage}$. It should be mentioned that using the two different biaxial damage coefficients in the formulation of the FSAM did not result in significant differences in model results obtained for all panel specimens investigated in this study.

2.6 Overview of the Working Principles of the FSAM
As described in the previous sections, the FSAM is merely a two-dimensional (plane-stress) constitutive model that relates the resultant stress state on reinforced concrete to the applied strain field, where an equivalent uniaxial stress–strain relationship for concrete (considering biaxial softening and hysteretic damage effects) is applied along fixed strut (crack) directions, a friction-based shear stress vs. sliding shear strain relationship is applied along crack surfaces, and a uniaxial stress–strain relationship is applied along reinforcement directions. Uniaxial stresses developing in concrete along two strut directions are superimposed with the shear stresses developing along crack surfaces and the uniaxial stresses developing in the reinforcing steel bars (smeared over concrete based on reinforcement ratios), in order to obtain the resultant stress field at a point. Instances of crack formation and crack directions are automatically calculated by the FSAM, based on the history of the applied strain field. The first crack is assumed to develop at the instant when the principal tensile strain first

exceeds the cracking strain of concrete, in perpendicular direction to that principal tensile strain. Upon load reversal, the second crack is assumed to develop in perpendicular direction to the first, at the instant when the tensile strain parallel to the first crack exceeds the concrete cracking strain. The FSAM does not require dimensions, definition of crack angles, definition of strut widths, or any other parameter that is not related to material stress vs. strain behavior (except a friction coefficient for the crack surfaces), and it can be implemented in any model formulation as a two-dimensional constitutive relationship representing the smeared stress vs. strain behavior of RC.

3 Comparison of Model Results with Experimental Data
With the mechanical principles and material constitutive relationships described in the previous section, the formulation of the FSAM was implemented in Matlab, together with a displacement-controlled iterative nonlinear analysis solution strategy (Clarke and Hancock 1990), in order to obtain the analysis results used for the experimental validation studies presented in this section.

Very few cyclic panel tests are available in the literature (Ohmori et al. 1989; Stevens 1987; Mansour 2001). Two different test programs were considered within the scope of this study. The first of these two test programs was conducted by Stevens (1987) using the "Shell Element Tester" facility at the University of Toronto and the other by Mansour (2001) using the "Universal Element Tester" facility at the University of Houston. Findings of these experimental programs have been used for development of the hysteretic panel model formulations proposed by Stevens et al. (1991) and Mansour and Hsu (2005). A more limited suite of comparisons between FSAM results and data obtained from these experiments were presented in the conference paper by Orakcal et al. (2012). Details of these experimental programs and results of comprehensive correlation studies conducted between model predictions and test measurements are presented in the following two sections.

For all panel specimens investigated, the constitutive material parameters used in the FSAM formulation were assigned values that match the as-tested properties of the materials used in the construction of the panel specimens, whenever material test results relevant to a specific parameter were reported. Whenever not, the material parameters were defined based on well-established empirical relationships provided in the literature. Thereby, a consistent methodology was used in selecting the material parameters for all panel specimens, as opposed to adjusting the material parameters (excluding the shear aggregate interlock friction coefficient; refer

Orakcal *et al. Int J Concr Struct Mater*   (2019) 13:51

Page 10 of 23

to Sect. 2.4) for optimizing the accuracy of the model in predicting the test results for an individual specimen. Accordingly, compressive strength of concrete in the FSAM was defined based on compression test results on samples of concrete used in the construction of the panel specimens. Empirical relationships by Chang and Mander (1994) and Saatcioglu and Razvi (1992) were used for generating the ascending and descending (post-peak) regions of the concrete compressive stress–stain envelope, respectively. The yield strength and strain hardening ratio parameters of the Menegotto and Pinto (1973) model were assigned values that represent the stress–strain curve obtained from tests on reinforcing steel bars used in the construction of the specimens. For all panels, the parameters controlling the cyclic stiffness degradation characteristics of the model (Fig. 2b) were defined as $R_0 = 20$, $a_1 = 18.5$, and $a_2 = 0.15$, as proposed originally by Menegotto and Pinto (1973). The behavioral parameters of the FSAM related to tension stiffening and concrete biaxial damage were defined as reported by the researchers who have conducted the tests, to best represent the experimentally-observed tension stiffening and biaxial damage characteristics of the test specimens, as also discussed in Sects. 2.5.4 and 2.5.5 of this paper.

3.1 Tests by Stevens (1987)

All of the panel tests by Stevens (1987) were conducted under stress control. Test panels were square, with 1625×1625 mm dimensions and 285 mm thickness. The test equipment was configured for loading principal (normal) stresses on the panel specimens. All panel reinforcement was arranged orthogonally in x and y directions, with reinforcement ratios ρ_x and ρ_y. Material properties, reinforcement ratios, and loading characteristics of the test program are listed in Table 1.

In this experimental program, there were two different parameters investigated; the loading type and reinforcement ratio. While specimens SE8 and SE10 were used to examine the effect of loading type on panel response (pure shear stress applied on SE8 and SE9; shear stress with proportionally-applied normal stresses $\sigma_x = \sigma_y = -|\tau_{xy}/3|$ applied on SE10), specimens SE8 and SE9 were utilized to investigate the effect of reinforcement ratio on the response ($\rho_x = 0.03$, $\rho_y = 0.01$ for SE8 and SE10; $\rho_x = \rho_y = 0.03$ for SE9).
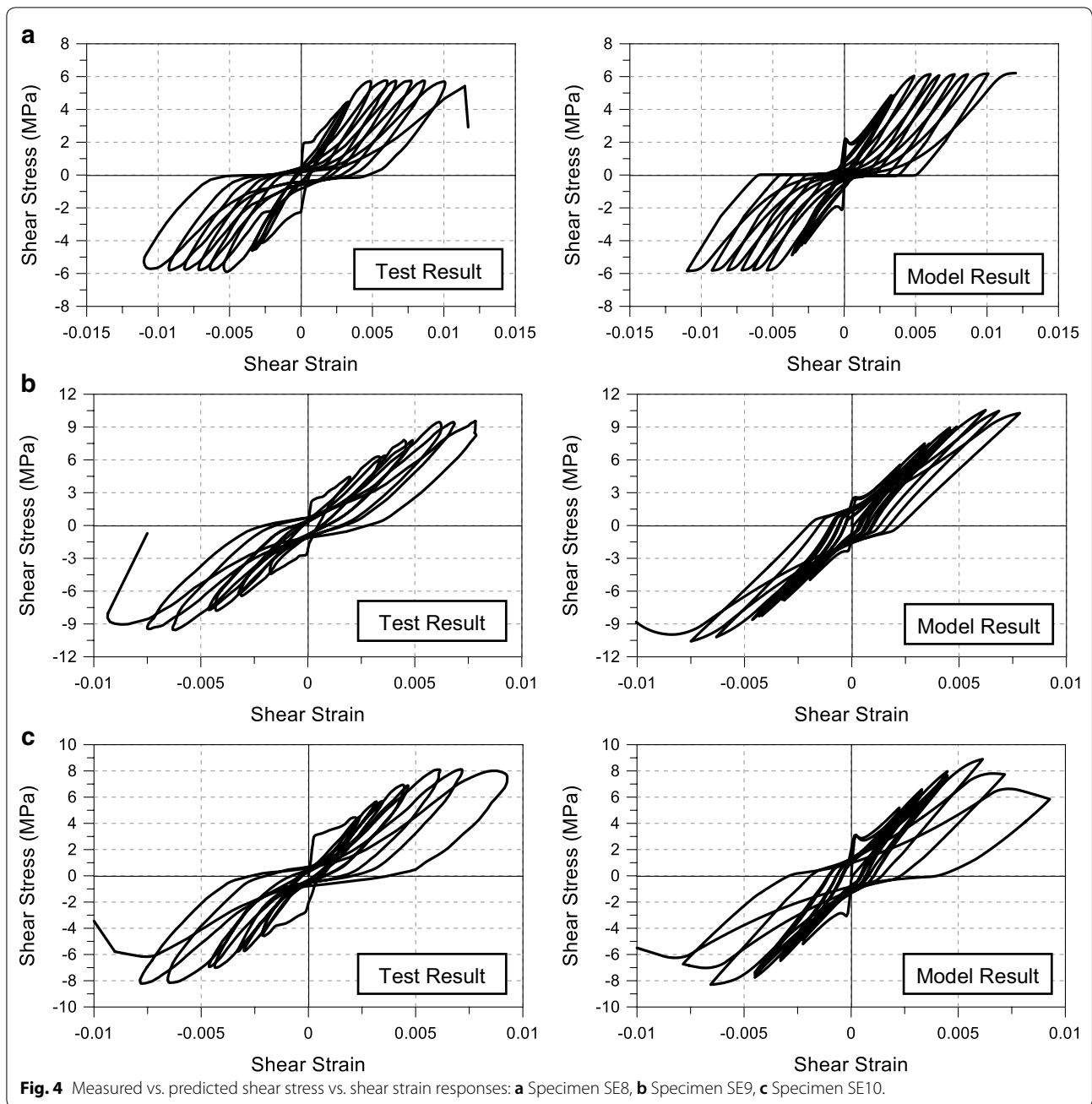
3.1.1 Global Response

In this section, the overall shear stress τ_{xy} vs. shear strain γ_{xy} behavior of the test specimens are compared with predictions of the FSAM.

Specimen SE8 The overall shear stress vs. shear strain behavior of Specimen SE8 is captured reasonably well by the FSAM (Fig. 4a). The shear stress capacity of the specimen, geometry of the loading and unloading curves, cracking shear stress level, and stiffness characteristics of the response are well-predicted. The FSAM overestimates the shear stress capacity of the specimen (average of the shear stress capacities in positive and negative loading directions) by only 2% of the test result. The experimentally-observed pinching behavior is clearly reflected in the model results. As a measure of hysteretic energy dissipation capacity, the cumulative area under the shear stress vs. strain loops predicted by the model corresponds to 76% of that of the measured response. Since Specimen SE8 had 1% reinforcement ratio in the y direction and 3% in the x direction, while the reinforcement in y direction yielded, the reinforcement in x direction remained linear elastic. Yielding of reinforcement in y direction not only limited the capacity, but also generated a ductile and highly-pinched shear stress vs. strain behavior for the specimen. The pronounced pinching behavior stems from yielding of reinforcing steel during the response of the specimen, leading to significant

Table 1 Panel test parameters, Stevens (1987).

Panel specimen:	SE8	SE9	SE10
Loading type:	$\sigma_x = 0$ $\sigma_y = 0$ τ_{xy} : *ReversedCyclic*	$\sigma_x = 0$ $\sigma_y = 0$ τ_{xy} : *ReversedCyclic*	$\sigma_x = -\left|\tau_{xy}/3\right|$ $\sigma_y = -\left|\tau_{xy}/3\right|$ τ_{xy} : *ReversedCyclic*
ρ_x	0.03	0.03	0.03
ρ_y	0.01	0.03	0.01
$f_{y,x}$ [MPa]	492	422	422
$f_{y,y}$ [MPa]	479	422	479
f'_c [MPa]	37	44	34
ε_{co}	0.0026	0.0026	0.0023
f_{ct} [MPa]	2.0	2.2	2.0
ε_t	0.0001	0.0001	0.00013

Orakcal *et al. Int J Concr Struct Mater*   (2019) 13:51

Page 11 of 23

Fig. 4 Measured vs. predicted shear stress vs. shear strain responses: **a** Specimen SE8, **b** Specimen SE9, **c** Specimen SE10.

widening of the cracks. Upon load reversal, the reinforcing steel that has yielded in tension counter-yields in compression, before the crack closes. During crack closure (during change in the sign of the shear strain applied on the specimen), the panel shear stress vs. strain behavior of the panel rapidly builds up stiffness, which results in the pinching behavior observed in both test results and model predictions.

Specimen SE9 General behavior of Specimen SE9 is captured by the model with reasonable accuracy (Fig. 4b). Although the shear stress capacity appears to

be slightly overestimated by the model (by 11% of the test measurement); pinching characteristics, cracking stresses, and cyclic stiffness properties of the behavior are all well-predicted (Fig. 4b). The widths of the loading and unloading loops in the stress–strain behavior are predicted to be only slightly narrower than the test results, with the cumulative area under the loops estimated at 88% of the experimentally-measured response. The main reason of this discrepancy may be attributed with variation in the cyclic behavior of concrete, which governs the overall response of this specimen.

As a measure of ductility, the shear strain capacity of the specimen (at which degradation in shear stress initiates), is well-estimated by the model, at approximately 95% of the test result. Since the specimen has 3% reinforcement in both directions, in the model for this specimen, the concrete compression struts are able to reach their maximum "softened and damaged" compressive stress capacity, prior to yielding of steel. However, since the tests were stress-controlled, none of these tests were continued until the failure mode of the specimens was clearly indentified.

Specimen SE10 Specimen SE10 was the one of the most important specimens of this test program, with its unequal reinforcement ratio in x and y directions, and with applied σ_x and σ_y compressive stresses which are both proportional to applied shear stress. Specimen SE10 is a replication of specimen SE8, with 1% reinforcement ratio in y direction and 3% reinforcement in x direction; the only difference being the compressive normal stresses (σ_x and σ_y) applied during testing. The shear stress capacity of this specimen is overestimated by only 5% of the test result (Fig. 4c). Other behavioral features of the response including cracking stress, stiffness of the loading and unloading curves, and pinching characteristics are predicted accurately. The model slightly overestimates the cumulative area under the shear stress vs. strain loops by 14% of the test result, and moderately underestimates the shear strain capacity of the specimen (at initiation of degradation in shear stress), at 80% of the test measurement in the negative loading direction.

Sensitivity to friction coefficient All model results presented in this paper for the specimens tested by Stevens (1987) are obtained using an optimal aggregate interlock friction coefficient value of $\eta = 0.1$. Modification of the interlock coefficient to a value of $\eta = 0.2$ [as used for the specimens by Mansour (2001)], results in approximately 30% increase in the shear stress capacity of Specimen SE8. For Specimen SE9, which is symmetrically-reinforced and subjected to a pure shear stress state, model results are not sensitive to the value of the friction coefficient, since shear strains do not develop along the cracks. In the case of Specimen SE10, although it is nonsymmetrically reinforced (similarly to SE8), the normal stresses applied on the specimen reduce the impact of the friction coefficient on the model response, yielding only 1% increase in the predicted shear stress capacity when the friction coefficient is increased from 0.1 to 0.2.
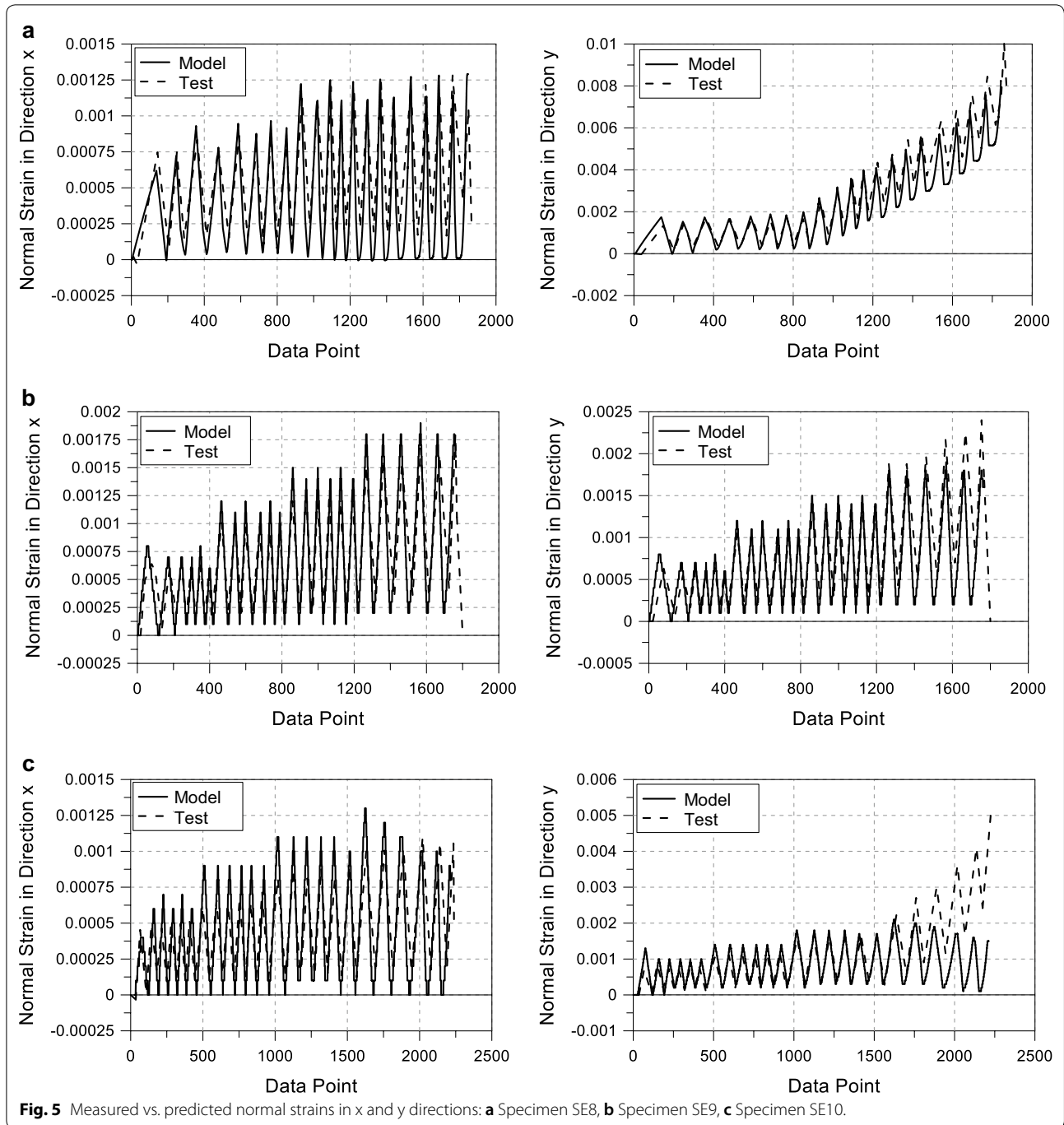
3.1.2 Local Responses

In this section, local response features including normal strains in x direction (Fig. 5), normal strains in y direction (Fig. 5), principal strain directions (Fig. 6), and concrete principal stress directions (Fig. 7) measured for all specimens by Stevens (1987) are compared with model results.

Specimen SE8 When the normal strains in x direction of Specimen SE8 are compared, it is observed that the strain history is predicted accurately by the model (Fig. 5a). Model predictions for the normal strains in y direction are also accurate. An increasing trend in strains in the y direction that starts at approximately the 900th step (corresponding to the first yield of reinforcement in y direction) can be clearly identified in both model and test results (Fig. 5b). When the principal strain directions are compared for Specimen SE8, as illustrated in Fig. 6a, the model accurately captures the measured principal strain direction history of the specimen, which changes noticeably throughout loading. Only a slight underestimation at the beginning of the analysis (for small shear strain values) is observed in the model results.
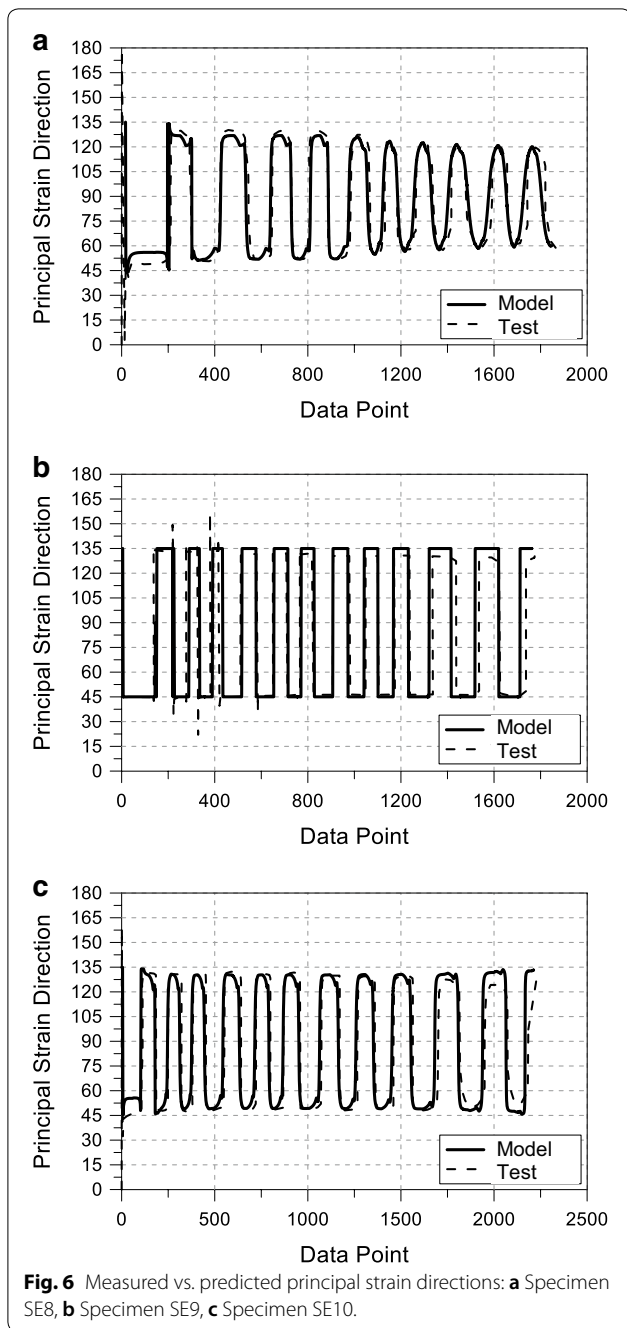
When the principal stress direction in concrete vs. panel shear stress behaviors are compared for Specimen SE8, it is observed that the model predictions for the principal stress direction in concrete do not significantly deviate from the two crack directions. As can be observed in Fig. 7a, the concrete principal stress direction in the model results undergoes marginal variation with the magnitude of the shear stress applied on the panel, due shear aggregate interlock stresses developing along crack surfaces, which deviate the principal stress directions from the two fixed crack directions. However, the variation is not significant, because the compressive stresses developing along the struts dominate over the shear stresses developing along the crack surfaces. There exists larger variation in the test measurements, probably due to a more complicated shear stress transfer mechanism across cracks; although these deviations are typically associated with unloading and reloading branches of the behavior, and the upper and lower bounds for the principal stress directions do not vary significantly with the magnitude of the shear stress (Fig. 7a). Thus, the model reasonably captures the experimental behavior with a friction-based model for shear aggregate interlock, maintaining its simplicity. It must be mentioned that the test result given in the figure is the envelope of the test measurements for the specimen, as the original graphic (Stevens 1987) was too congested for digitizing purposes.

The test results presented in Figs. 6a, 7a clearly demonstrate that for this specimen, although the principal strain direction noticeably changes with loading (under increasing strains), the direction of principal stresses in concrete do not deviate significantly from the two crack directions. This behavior is clearly captured in the model results, since the model does not follow the assumption that principal strain and concrete principal stress directions coincide.
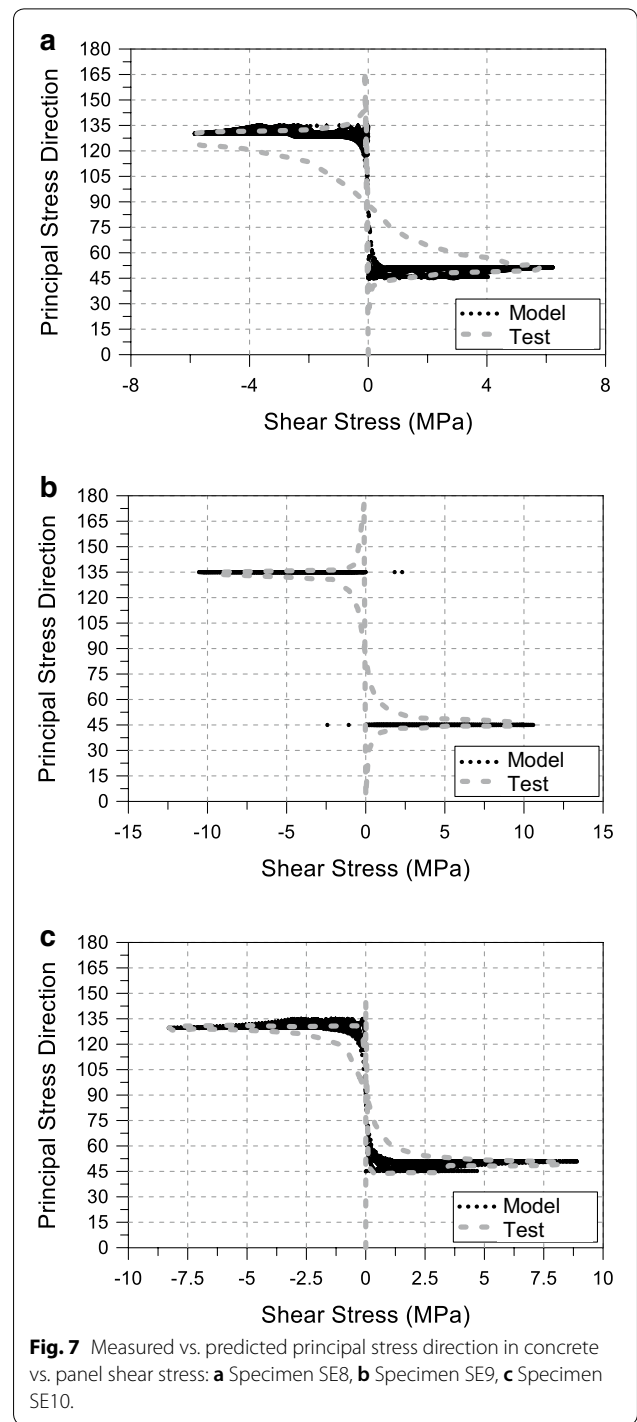
Fig. 5 Measured vs. predicted normal strains in x and y directions: **a** Specimen SE8, **b** Specimen SE9, **c** Specimen SE10.

Specimen SE9 When the normal strains in the x direction are compared for Specimen SE9, it is observed that the general ascending trend is captured by the model (Fig. 5b). The general ascending trend in normal strains in y direction is again captured, with increasing discrepancies at later stages of loading (Fig. 5b). At this point, it should be clarified that the normal strains predicted by the model in x and y directions are approximately identical. Considering that the specimen had equal reinforcement ratios in both directions and pure shear loading is applied, the model predictions are mechanically consistent. Therefore, differences between normal strains measured in the x and y directions during the test may be attributed to imperfections in the test conditions. When the principal strain directions are compared for this specimen, as depicted in Fig. 6b, test results are

Fig. 6 Measured vs. predicted principal strain directions: **a** Specimen SE8, **b** Specimen SE9, **c** Specimen SE10.

Fig. 7 Measured vs. predicted principal stress direction in concrete vs. panel shear stress: **a** Specimen SE8, **b** Specimen SE9, **c** Specimen SE10.

well-predicted by the model. Model predictions for the principal strain directions are 45° and 135°, since the pure shear stress state applied on the symmetrically-reinforced specimen creates a pure shear strain state, which is also observed in the test measurements. Furthermore, under the pure shear stress state applied on the panel specimen, because of identical reinforcing steel ratios and yield strengths along the two reinforcement directions, concrete is also subjected to a pure shear stress state.

Therefore, the principal stress directions in concrete and the fixed crack directions coincide at 45° and 135° angles during the entire loading history, which is also in agreement with the test results, as shown in Fig. 7b.

Specimen SE10 For specimen SE10, when the normal strains in x direction are compared, it is observed that the

general response is reasonably captured (Fig. 5c). When the normal strains in y direction are compared, it is seen that the general trend is captured for most of the loading history, with increasing discrepancies at later stages of loading (Fig. 5c), probably due to degradation in the overall shear stress vs. strain behavior predicted by the model. When the principal strain directions are compared, as shown in Fig. 6c, the test measurements are predicted accurately by the model. The measured and predicted principal stress directions in concrete (vs. shear stress on the panel) are compared in Fig. 7c. Similarly to Specimen SE8, variation in the principal stress directions predicted by the model are not significant, because of larger concrete compressive stresses developing along the struts compared to smaller shear friction stresses developing along the crack surfaces. There is slightly more variation in the experimentally-measured principal stress directions; however, as shown in Fig. 7c, such variation is typically limited to the unloading and reloading branches of the response, at regions of small shear stress. At regions of high shear stress, the measured principal stress directions do not vary significantly, and are in good agreement with model predictions, validating the modeling approach used.

3.2 Tests by Mansour (2001)

There are two important characteristics of the experimental program by Mansour (2001). First, these tests (12 full-size reversed cyclic panel tests) were performed under strain control, which revealed the sudden stiffness drop as an effect of first cracking on panel response, as well as degradation in shear stress during later stages of loading due to the behavior of concrete in compression. Second, the test program was aimed to investigate the effect of reinforcement ratio to the overall behavior (i.e., $\rho_x = \rho_y = 0.0077$ for CA2; $\rho_x = \rho_y = 0.017$ for

CA3; $\rho_x = \rho_y = 0.027$ for CA4), asymmetry of reinforcement ratio in the orthogonal directions (i.e., $\rho_x = 0.017$, $\rho_y = 0.0077$ for CB3; $\rho_x = 0.027$, $\rho_y = 0.0067$ for CB4) and different loading conditions (i.e., pure shear stress on CA2, normal and shear stresses on CD4, and normal stresses on CE4).

The orientation of reinforcement was a test variable in this experimental program in order to generate the different loading conditions. Thus, a selection of 7 specimens (CA2, CA3, CA4, CB3, CB4, CD4, and CE4), among the total of 12, that capture the various test variables were considered within the scope of this study. All of these panel specimens had 1397×1397 mm dimensions and 178 mm thickness. The testing was configured for application of principal (normal) strains to the test specimens at different angles, resulting in pure shear stress (CA and CB series—reinforcement at 45° relative to external loading), in pure normal stresses (CE series—reinforcement parallel to external loading) and combined normal and shear stresses (CD series—X reinforcement at 68.2° relative to one of the external loading directions). Material properties, steel reinforcing ratios, and loading characteristics of the test specimens are described in Table 2.
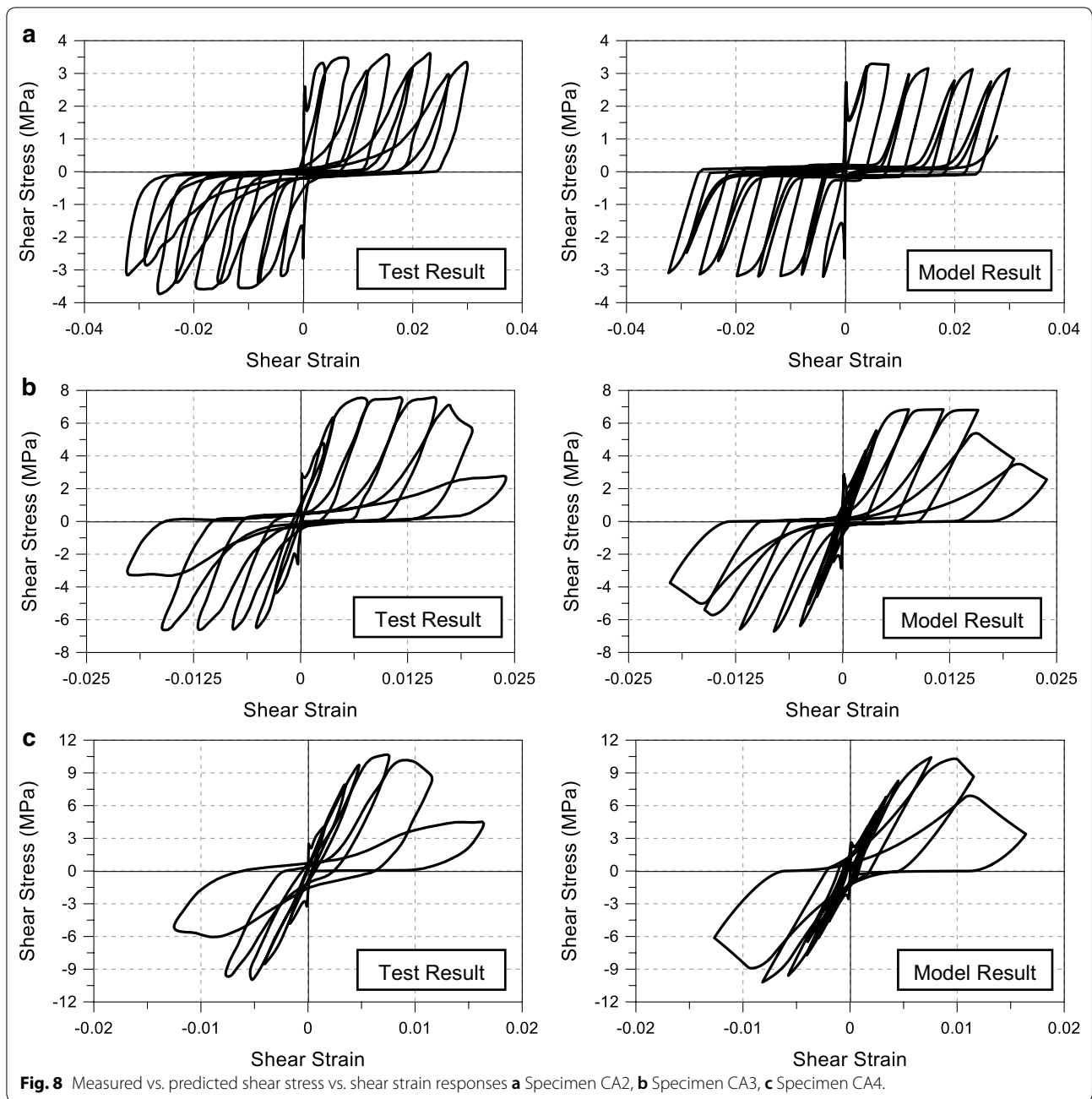
3.2.1 Global Response

In this section, the overall shear stress τ_{xy} vs. shear strain γ_{xy} behavior of the selected test specimens are compared with model results.

Specimen CA2 Specimen CA2 has the smallest reinforcement ratio in both directions, with a value of 0.77%. When test results are compared with model predictions, the model is observed to slightly underestimate the shear stress capacity of the specimen, at 88% of the measured value. Other features of the response including the shapes of the unloading and reloading curves, stiffness characteristics, cracking stress values, and pinching behavior

Table 2 Panel test parameters, Mansour (2001).

Panel specimen:	CA2	CA3	CA4	CB3	CB4	CD4	CE4
Loading type:	$\sigma_x = 0$ $\sigma_y = 0$ $\tau_{xy} : RC$	$\sigma_x = 0$ $\sigma_y = 0$ $\tau_{xy} : RC$	$\sigma_x = 0$ $\sigma_y = 0$ $\tau_{xy} : RC$	$\sigma_x = 0$ $\sigma_y = 0$ $\tau_{xy} : RC$	$\sigma_x = 0$ $\sigma_y = 0$ $\tau_{xy} : RC$	$\sigma_x = 1.05\tau_{xy}$ $\sigma_y = -1.05\tau_{xy}$ $\tau_{xy} : RC$	$\sigma_x = RC$ $\sigma_y = -\sigma_x$ $\tau_{xy} = 0$
ρ_x	0.0077	0.017	0.027	0.017	0.027	0.02	0.019
ρ_y	0.0077	0.017	0.027	0.0077	0.0067	0.02	0.019
$f_{y,x}$ [MPa]	424	425	453	425	453	453	453
$f_{y,y}$ [MPa]	424	425	453	424	424	453	453
f'_c [MPa]	45	44.5	45	48	47	43	47
ε_{co}	0.0025	0.0024	0.0028	0.0026	0.0024	0.0024	0.0022
f_{ct} [MPa]	2.1	2.1	2.1	2.2	2.2	2.1	2.2
ε_t	0.00008	0.00008	0.00008	0.00008	0.00008	0.00008	0.00008

RC reversed cyclic.

Fig. 8 Measured vs. predicted shear stress vs. shear strain responses **a** Specimen CA2, **b** Specimen CA3, **c** Specimen CA4.

(to some extent) are captured with reasonable accuracy (Fig. 8a). The hysteretic energy dissipation capacity of the specimen, defined as the cumulative area under the shear stress vs. strain loops, is underestimated by the model at 68% of the test measurement, due to the narrower loops in the model prediction. Since the specimen has relatively low amount of reinforcement in both directions, the behavior is dominated by yielding of reinforcing steel in both test results and model predictions.

Specimen CA3 Specimen CA3 has a reinforcement ratio of 1.7% in both directions. The analytical model accurately predicts the overall shear stress vs. shear strain behavior of this specimen in terms of its stiffness, cracking stress, and pinching attributes (Fig. 8b). The shear stress capacity of the specimen is underestimated by only 5% of the test result. The difference between model and test results is mostly associated with the shape of the envelope of the response, which was found to be influenced both by the shape of the concrete stress–strain

Orakcal *et al. Int J Concr Struct Mater*   (2019) 13:51

Page 17 of 23

behavior in compression and the effective yield strength of reinforcing steel. The cumulative area under the shear stress vs. strain loops estimated by the model corresponds to 82% of the test result, and the model predicts the shear strain capacity of the specimen (at initiation of shear stress degradation) at 88% of the measured value.

Specimen CA4 Specimen CA4 had the largest reinforcement ratio, with the value of 2.7% in both directions. The model well-predicts the overall shear stress vs. shear strain behavior of this specimen well, with slight discrepancies in cyclic stiffness characteristics. Features including the pinching effect, cracking stress, and shear stress capacity are all captured accurately (Fig. 8c). The shear stress capacity of the specimen is captured with 100% accuracy, and its shear strain capacity (at initiation of shear stress degradation) is overestimated by only 7% of the test measurement. The model also well-predicts the cumulative area under the measured shear stress vs. strain loops for the specimen, at 96% of the test result. The shape of the envelope of the predicted response was found to be significantly influenced by the shape of the concrete stress–strain behavior in compression.

Specimen CB3 CB-series specimens were subjected to the same loading conditions as the CA series (pure shear). Specimen CB3 incorporated asymmetric reinforcement, and the overall response predicted by the model appears to be governed by yielding of reinforcement in y direction, with the lower reinforcement ratio (Fig. 9a). The hysteretic shape of the analytical response is considerably different than that of the experimentally-measured, as the test result shows a shape that seems to be influenced in-part by the concrete stress–strain behavior in compression. The model does not capture the degradation in shear stress at high shear strains, and predicts the cumulative area under the shear stress vs. strain loops at only 60% of the test measurement. Nevertheless, the shear stress capacity of the specimen is well-captured by the model, at 96% of the measured capacity.

Specimen CB4 Specimen CB4 was similar to CB3, but with a larger reinforcement ratio in the x direction, which made the shape of the experimentally-measured response even more influenced by the concrete stress–strain behavior in compression (Fig. 9b). Similar discrepancies between model and test results to those observed for specimen CB3 are observed for this specimen. Although the model well-predicts the shear stress capacity of the specimen, at 99% of the measured capacity, it does not capture the degradation in shear stress at high shear strains, and the cumulative area under the shear stress vs. strain loops predicted by the model corresponds to 64% of the test result.

Specimen CD4 CD-series specimens were subjected to the most complex loading configuration, with normal and shear stresses applied simultaneously. The model slightly underestimates the shear stress capacity of specimen CD4 by only 10% of the measured; however, similar discrepancies (to those observed for specimens CB3 and CB4) related to the hysteretic shape of the behavior are observed, although to a lesser degree (Fig. 9c). Differently for this specimen, the model captures degradation in shear stress (in the positive loading direction) associated with crushing of concrete, albeit at a much larger shear strain compared to the test result. The cumulative area under the shear stress vs. strain loops is again underestimated by the model, at 61% of measured response.

The experimentally-observed failure (strength degradation) mode of specimens CB3, CB4, and CD4 (Fig. 9a–c) was crushing of concrete along compression struts, after yielding of reinforcement. Therefore, the most probable reason why the FSAM did not capture the degradation associated with concrete crushing (Fig. 9a, b), or predicted initiation of degradation a higher shear strain than measured (Fig. 9c), is the relatively simple "compression softening" model implemented in its formulation to represent softening in the compressive stress–strain behavior of concrete along the principal compression direction, due to presence of large tensile strains in the perpendicular direction. As described in Sect. 2.5.3 of this paper, the so-called "Model B" by Vecchio and Collins (1993), which considers reduction only in the concrete compressive stresses, was adopted in the FSAM formulation, since it is more suitable for a hysteretic panel model formulation. It is believed that implementation of a more robust compression softening model, which also considers reduction in the strain at peak compressive stress on the monotonic stress vs. strain envelope of concrete (strain softening behavior), such as "Model A" by Vecchio and Collins (1993), may improve the ductility predictions of the FSAM for these particular specimens. However, Model A is not suitable for hysteretic implementation, unless ad-hoc manipulations are made to convert its monotonic nature into a hysteretic one.

Specimen CE4 CE-series specimens were subjected to loading (normal stresses) parallel to the reinforcement directions. The model for specimen CE4 model recovers most features observed in the experimental response (stiffness, strength, hysteretic response), which is governed by the uniaxial stress vs. strain behavior of the reinforcing steel bars (Fig. 9d). The shear stress capacity and the cumulative area under the stress vs. strain loops predicted by the model for this specimen correspond to 100% and 99% of the experimentally-measured values, respectively, which validates the reliability of the uniaxial stress–strain model implemented in the FSAM for reinforcing steel.
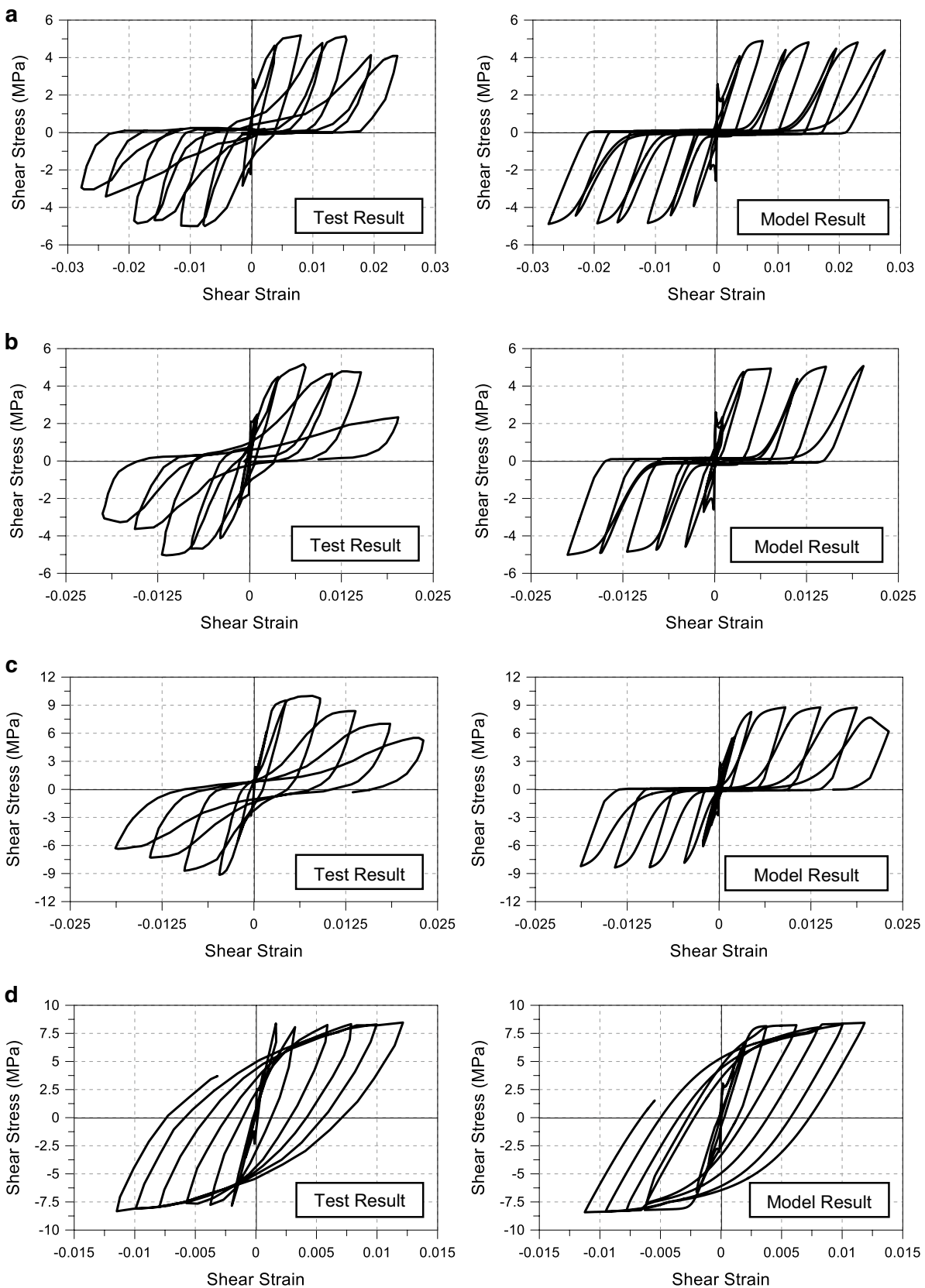
Fig. 9 Measured vs. predicted shear stress vs. shear strain responses **a** Specimen CB3, **b** Specimen CB4, **c** Specimen CD4, **d** Specimen CE4.

Orakcal *et al. Int J Concr Struct Mater*   (2019) 13:51

Page 19 of 23

Sensitivity to friction coefficient All model results presented for the test specimens by Mansour (2001) are generated using an optimal aggregate interlock friction coefficient value of η = 0.2. Similarly to the tests by Stevens (1987), modification of the friction coefficient noticeably changes the analytical response obtained for some of these specimens. For specimen CA2, CA3, CA4, and CE4, model results are not sensitive to the friction coefficient, due to the loading conditions imposed on these specimens and symmetry of the reinforcement. Differences in model results are observed for Specimens CB3, CB4, and CD4. Reduction of the coefficient to a value of η = 0.1 [as used for the specimens by Stevens (1987)], results in approximately 20% and 25% decrease in the shear stress capacity of Specimens CB3 and CB4, respectively Interestingly for Specimen CD4, which was subjected to the complex loading condition, reducing the friction coefficient to a value of 0.1 does not significantly change the predicted shear stress capacity of the specimen, but decreases the shear strain at which shear stress degradation initiates by approximately 20%.

Similarly to the discrepancy in tension stiffening behavior observed in these two experimental programs (Bentz 2005), the necessity of using different interlock friction coefficients to obtain the best correlation between model and test results for the two programs can be attributed to different shear aggregate interlock characteristics of the specimens, such as the mean aggregate size used in the concrete mix. Recent studies on implementation of the FSAM into finite element formulations for modeling of RC walls (Gullu and Orakcal 2019; Gullu et al. 2019) have shown that using a coefficient of η = 0.5 consistently provided accurate response predictions for numerous RC wall specimens that were tested as part of multiple experimental programs, where the dimensions of the wall specimens were significantly larger than the panel specimens analyzed in the present study. This variation is most likely due to the different characteristics of concrete (particularly the mean aggregate size) used in the construction of these larger wall specimens, as well as more non-uniform internal stress distributions and crack orientations developing on the walls. For modeling of real-life walls, adopting a larger value (e.g., η = 0.5) for the friction coefficient therefore seems more reasonable.

3.2.2 Local Responses

In this section, normal strains measured in x and directions of representative test specimens are compared with model predictions. Since the reinforcement ratios were same in both directions for the CA-series specimens, it is expected that the normal strains in x and y directions should be approximately equal, when the specimens are subjected a state of pure shear stress. The model results consistently show this type of behavior, similarly to the test results for the CA specimens, although some differences are observed during the last cycles (Fig. 10a, b). When the model and test results are compared, the strain predictions in both x and y directions are reasonable for both specimens CA2 and CA3, but the residual (plastic) strains at the end of the test estimated by the model are consistently lower than the test results.

Specimens CB4 and CD4 incorporated asymmetry either in reinforcement ratios or loading conditions, resulting in asymmetry in the normal strains observed in x and y directions (Fig. 10c, d). A similar situation is observed for the strain histories predicted by the model. In general, the progression of residual strain, as well as the maximum strain values attained during each cycle or incursions into negative (compressive) values, are well captured.

4 Overview of FSAM Implementation in Structural Models

Since the FSAM is intended to simulate the smeared stress vs. average strain behavior of reinforced concrete under generalized plane stress loading, it is suitable for implementation in model formulations for simulating the in-plane nonlinear behavior of reinforced concrete walls, in which the constitutive model elements are membrane elements. The FSAM can also be used to construct a shell element formulation, using a layered membrane assembly.

Research has been conducted on implementation of the FSAM into a "macro-fiber" model formulation [SFI-MVLEM, Shear Flexure Interaction Multiple Vertical Line Element Model (Kolozvari et al. 2015b, c, 2018a, c, 2019b)] for simulating the coupled axial-shear-flexural responses of reinforced concrete walls or columns, where the uniaxial line elements in a fiber model formulation were replaced with membrane elements, the plane-stress vs. strain behavior of which were described with FSAM. Accordingly, axial and shear stress vs. strain responses of each fiber were coupled, which further allowed capturing of the experimentally-observed coupling of axial-shear-flexural responses in reinforced concrete walls or columns, through a fiber model formulation. Detailed information on implementation of the FSAM in the computational platform OpenSees [http://opensees.berkeley.edu] as a plane-stress material model (*nDMaterial FSAM*) used within the macro-fiber model formulation SFI-MVLEM, is provided by Kolozvari et al. (2015a, 2018c). Results of earthquake response history analyses
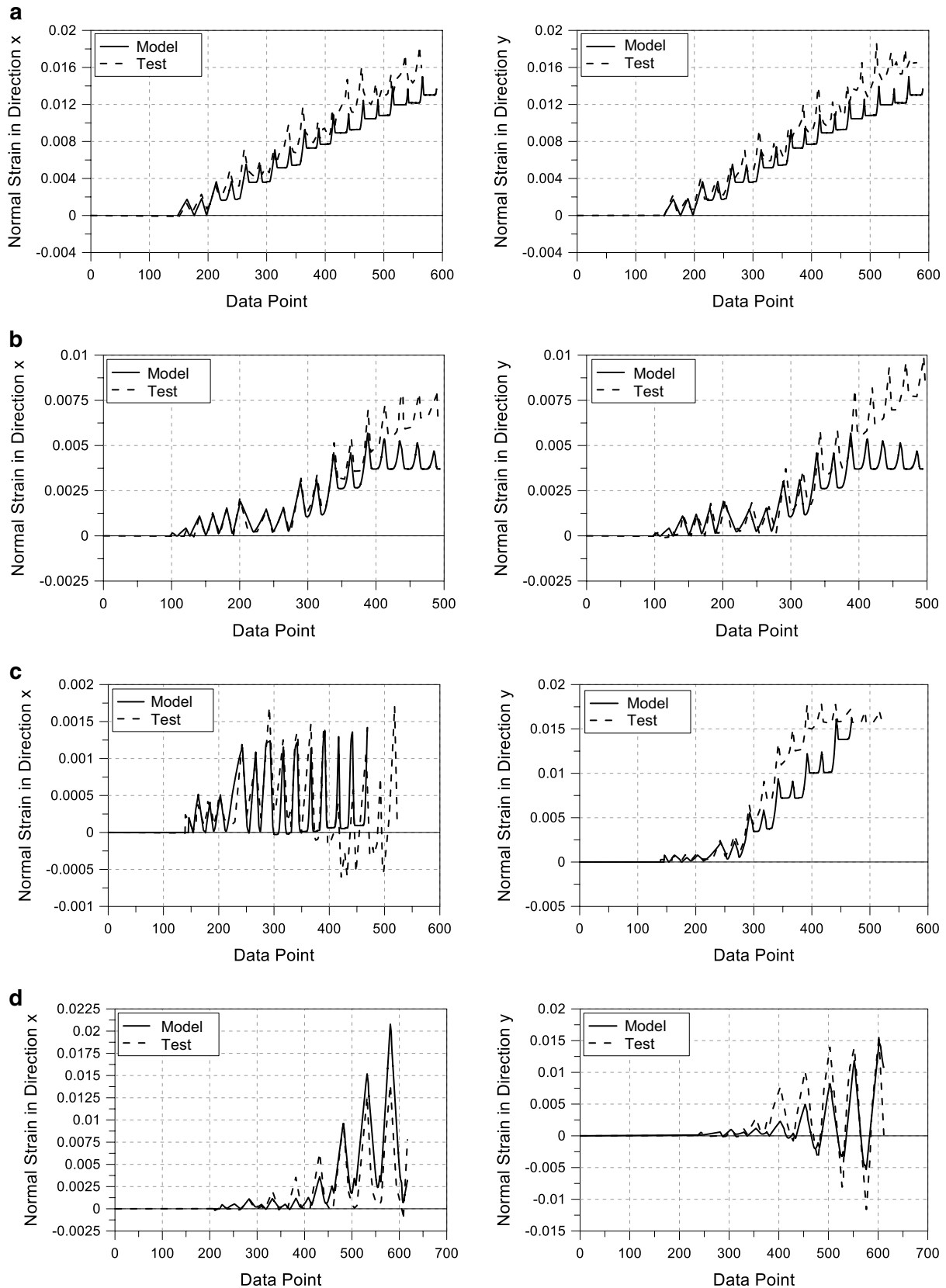
Fig. 10 Measured vs. predicted normal strains in x and y directions: **a** Specimen CA2, **b** Specimen CA3, **c** Specimen CB4, **d** Specimen CD4.

Orakcal *et al. Int J Concr Struct Mater*   (2019) 13:51

Page 21 of 23

on wall-frame assemblies and coupled wall systems (Kolozvari et al. 2018d; Kolozvari and Wallace 2016), in which the FSAM was used within the SFI-MVLEM formulation adopted for the walls, have also shown that the FSAM is capable of providing computationally-stable and accurate response predictions for coupled walls or wall-frame systems subjected to dynamic loading.

Recent studies (e.g., Gullu and Orakcal 2019; Gullu et al. 2018, 2019; Kolozvari et al. 2018b, 2019a) have focused on adopting the FSAM in finite element model formulations for walls, using four-node quadrilateral membrane or shell elements, the in-plane stress vs. strain behavior of which are described by the FSAM. Considering contemporary needs towards improving seismic design and performance-based assessment procedures, a reliable analysis model should be able to capture, with a reasonable level of accuracy, important response characteristics of walls with various behavioral characteristics (e.g., flexure-controlled, shear controlled, various levels of shear–flexure interaction, sliding shear, etc.), at both global (load vs. displacement) and local (e.g., strain) response levels, under generalized loading conditions. Towards this goal, current state-of-the-art rapidly progresses towards nonlinear finite element modeling of walls. Finite element modeling inherently considers numerous important aspects of wall behavior pertaining to performance-based seismic design, including characterization of nonlinear shear behavior, consideration of coupled shear and flexural responses, plane sections not remaining plane due to shear deformations, definition of a cracked shear stiffness, and coupling of fluctuating axial load with wall shear capacity. All of these aspects are real-life issues that are presently being discussed among the research and engineering community, towards improvement of design applications and performance-based assessment procedures for wall buildings. Finite element modeling methodologies to be used for such practical purposes must incorporate constitutive model formulations that depend on well-defined parameters related to physical behavior, so that the model can be understood and calibrated by the engineer using it. This has been the primary motivation behind development of the FSAM. As described in this paper, the formulation of the FSAM is based on clear assumptions (crack directions are fixed, cracks are perpendicular, concrete along struts follows a uniaxial stress–strain relationship, shear stress transfer across cracks is friction-based), with as few ad-hoc model parameters (e.g., friction coefficient) as possible. Other than its inherent assumptions, mechanical principles of the FSAM are based purely on physical material behavior, which can be updated as more information on material stress–strain behavior becomes available.

5 Summary and Conclusions

An original constitutive model formulation (named as the Fixed Strut Angle Model—FSAM) was developed for simulating the hysteretic axial/shear behavior of reinforced concrete (RC) panel (membrane) elements. The formulation of the FSAM follows a fixed-crack-angle modeling approach, and its working principles are based on interpretation and simplification of previous modeling methodologies presented in the literature. In this paper, the model formulation was described in detail and results of correlation studies were presented, for a comprehensive experimental validation of the FSAM against panel tests results available in the literature. A significant and unique aspect of this study is that the FSAM was extensively validated at various response levels (shear stress vs. strain behavior, normal strains, principal strain directions, and concrete principal stress directions) using experimental data obtained from two different panel test programs. Based on the analytical results presented in this study, the following conclusions on the characteristics of the FSAM can be reached:

- The FSAM has proven to be a relatively simple constitutive model that is capable of simulating the coupled axial/shear stress–strain behavior of reinforced concrete panel elements. Despite its simple formulation and well-defined assumptions, results of the correlation studies conducted in this paper indicate that the FSAM consistently provides reasonably accurate response predictions for RC panels with various reinforcement configurations, subjected to various loading conditions (stress states). The model was shown to generally capture the overall behavioral attributes of most of the RC panel specimens investigated, including the overall shear stress vs. shear strain behavior, cracking shear stress, shear stiffness, cyclic stiffness degradation, ductility, pinching behavior, and failure mode (crushing of concrete vs. yielding of reinforcement).

- Comparison of the overall shear stress vs. shear strain responses reveal the FSAM provides shear stress capacity predictions with an error margin of approximately $\pm 10\%$ of the test results, when a shear aggregate interlock friction coefficient of 0.1 was used for all specimens tested by Stevens (1987) and 0.2 for all specimens tested by Mansour (2001). The friction coefficient remains as the only ad-hoc parameter of the model, and is believed to be sensitive to parameters of test specimens associated with the shear aggregate interlock characteristics of the crack surfaces, such as the mean aggregate size used in the concrete mix.

Orakcal *et al. Int J Concr Struct Mater*   (2019) 13:51

Page 22 of 23

- Averaged over all panel specimens investigated in this paper, the shear stress capacity prediction of the FSAM corresponds to 98% of the experimentally-measured capacity of the specimens, whereas the hysteretic strain energy dissipation capacity prediction of the FSAM (defined as the cumulative area under the hysteretic shear stress vs. strain loops) corresponds to 81% of the measured. The FSAM was not able to accurately capture the ductility characteristics of the measured shear stress vs. strain responses (characterized by the shear strain at initiation of degradation in shear stress) for only three (CB3, CB4, CD4) of the ten panel specimens considered, possibly due to simplifications in behavioral modeling of compression softening effects on concrete.
- The FSAM was also shown to be capable of providing accurate predictions of local deformations for the specimens investigated, including normal strains in two orthogonal directions, the direction of principal strains developing in the panel element, and the direction of principal stresses developing in concrete. The experimental observation that even when the principal strain directions rotate during loading, the direction of principal stresses in concrete do not deviate significantly from the two crack directions, is captured by the FSAM.
- The flexible formulation of the FSAM allows revisions including implementation of different constitutive material models and various shear stress transfer mechanisms across cracks, as well as incorporation of different compression softening, tension stiffening, and biaxial damage parameters. However, the state-of-the-art constitutive material models used in this study for concrete and reinforcing steel have been shown to be satisfactory in simulating the material behavior and failure modes of the RC panels investigated.

With the features and potential improvements described in this paper, the FSAM is believed to provide a good balance between simplicity and accuracy in simulating nonlinear RC behavior under plane-stress loading conditions. Formulation of the FSAM has been implemented in the open-source computational platform OpenSees (http://opensees.berkeley.edu) as an efficient and flexible constitutive model that can be used for response prediction RC walls with various behavioral characteristics (flexure-controlled, shear controlled, or shear–flexure interaction responses), under seismic actions. Current studies focus on seismic response simulation of RC walls and wall systems using either macroscopic or finite element modeling approaches, in which the FSAM is used to describe the constitutive behavior of the model elements.

Authors' contributions
KO and LMM jointly developed and coded the FSAM formulation. DU conducted the analyses, using the FSAM, of the panel specimens investigated. All authors read and approved the final manuscript.

Author details
[1] Dept. of Civil Engineering, Bogazici University, 34342 Bebek, Istanbul, Turkey. [2] Dept. of Civil Engineering, University of Chile, Santiago, Chile.

References
Belarbi, A., & Hsu, T. C. (1994). Constitutive laws of concrete in tension and reinforcing bars stiffened by concrete. *ACI Structural Journal, 91*(4), 465–474.

Belarbi, A., & Hsu, T. C. (1995). Constitutive laws of softened concrete in biaxial tension compression. *ACI Structural Journal, 92*(5), 562–573.

Bentz, E. C. (2005). Explaining the riddle of tension stiffening models for shear panel experiments. *ASCE Journal of Structural Engineering, 131*(9), 1422–1425.

Chang, G. A., & Mander, J. B. (1994). *Seismic energy based fatigue damage analysis of bridge columns: Part I-evaluation of seismic capacity*. NCEER Report No. 94-0006, National Center for Earthquake Engineering Research.

Clarke, M. J., & Hancock, G. J. (1990). A study of incremental-iterative strategies for non-linear analyses. *International Journal for Numerical Methods in Engineering, 29,* 1365–1391.

Filippou, F. C., Popov, E.G., & Bertero, V.V. (1983). *Effects of bond deterioration on hysteretic behavior of reinforced concrete joints*. EERC Report No. UCB/EERC-83/19. Berkeley: University of California.

Gérin, M., & Adebar, P. (2009). Simple rational model for reinforced concrete subjected to seismic shear. *ASCE Journal of Structural Engineering, 135*(7), 753–761.

Gullu, M. F., & Orakcal, K. (2019). Nonlinear finite element modeling of reinforced concrete walls with varying aspect ratios. *Journal of Earthquake Engineering*. https://doi.org/10.1080/13632469.2019.1614498.

Gullu, M. F., Orakcal, K., & Kolozvari, K. (2018). Nonlinear finite element modeling of low-rise shear-controlled structural walls. In *Proceedings, 16th European Conference on Earthquake Engineering*. Thessaloniki, Greece

Gullu, M. F., Orakcal, K., & Kolozvari, K. (2019). The Fixed-Strut-Angle Finite Element (FSAFE) model for reinforced concrete structural walls. *Bulletin of Earthquake Engineering*. https://doi.org/10.1007/s10518-019-00641-0.

Hsu, T. C., & Zhu, R. H. (2002). Softened membrane model for reinforced concrete elements in shear. *ACI Structural Journal, 99*(4), 460–469.

Kashani, M. M., Lowes, L. N., Crewe, A. J., & Alexander, N. A. (2015). Phenomenological hysteretic model for corroded reinforcing bars including inelastic buckling and low-cycle fatigue degradation. *Computers & Structures, 156,* 58–71.

Kolozvari, K., Arteta, C., Fischinger, M., Gavridou, S., Hube, M., Isakovic, T., et al. (2018a). Comparative study of state-of-the-art macroscopic models for planar reinforced concrete walls. *ACI Structural Journal, 115*(6), 1637–1657.

Kolozvari, K., Biscombe, L., Dashti, F., Dhakal, R. P., Gogus, A., Gullu, M. F., et al. (2019a). State-of-the-art in nonlinear finite element modeling of isolated planar reinforced concrete walls. *Engineering Structures, 194,* 46–65.

Kolozvari, K., Kalbasi, K., Orakcal, K., Massone, L. M., & Wallace, J. W. (2019b). Shear–flexure-interaction models for planar and flanged reinforced concrete walls. *Bulletin of Earthquake Engineering*. https://doi.org/10.1007/s10518-019-00658-5.

Kolozvari, K., Miller, R., Gullu, M. F., & Orakcal, K. (2018b). Three-dimensional finite element modeling of reinforced concrete walls under uniaxial and biaxial loading. In *Proceedings, 16th European Conference on Earthquake Engineering*. Thessaloniki, Greece.

Kolozvari, K., Orakcal, K., & Wallace, J. W. (2015a). *Shear–flexure interaction modeling for reinforced concrete structural walls and columns under reversed cyclic loading*. PEER Technical Report No: PEER 2015/12. University of California Berkeley.

Kolozvari, K., Orakcal, K., & Wallace, J. W. (2015b). Modeling of cyclic shear–flexure interaction in reinforced concrete structural walls I: Theory. *ASCE Journal of Structural Engineering, 141*(5), 04014135.

Kolozvari, K., Orakcal, K., & Wallace, J. W. (2018c). New OpenSees models for simulation of nonlinear flexural and shear–flexural interaction behavior of reinforced concrete walls and columns. *Computers & Structures, 196,* 246–262.

Kolozvari, K., Terzic, V., Miller, R. J., & Saldana, D. (2018d). Assessment of dynamic behavior and seismic performance of a high-rise RC coupled wall building. *Engineering Structures, 176,* 606–620.

Kolozvari, K., Tran, T. A., Orakcal, K., & Wallace, J. W. (2015c). Modeling of cyclic shear–flexure interaction in reinforced concrete structural walls II: Experimental validation. *ASCE Journal of Structural Engineering, 141*(5), 04014136.

Kolozvari, K., & Wallace, J. W. (2016). Practical nonlinear modeling of reinforced concrete structural walls. *ASCE Journal of Structural Engineering, 142*(12), G4016001.

Mansour, M. Y., & Hsu, T. C. (2005). Behavior of reinforced concrete elements under cyclic shear. *ASCE Journal of Structural Engineering, 131*(1), 54–65.

Mansour, M. Y., Hsu, T. C., & Lee, J. Y. (2002). Pinching effect in hysteretic loops of R/C shear elements. *ACI Special Publication, 205,* 293–321.

Mansour, M. Y. (2001). *Behavior of reinforced concrete elements under cyclic shear: Experiments to theory* (Ph.D. thesis). Department of Civil Engineering, University of Houston.

Massone, L. M., & López, E. E. (2014). Modeling of reinforcement global buckling in RC elements. *Engineering Structures, 59,* 484–494.

Massone, L. M., & Moroder, D. (2009). Buckling modeling of reinforcing bars with imperfections. *Engineering Structures, 31*(3), 758–767.

Matlab. MathWorks, Natick, MA.

Menegotto, M., & Pinto, E. (1973). Method of analysis for cyclically loaded reinforced concrete plane frames including changes in geometry and non-elastic behavior of elements under combined normal force and bending. In *Proceedings, IABSE Symposium*. Lisbon, Portugal.

Ohmori, N., Takahashi, T., Inoue, N., Kurihara, K., & Watanabe, S. (1989). Experimental studies on nonlinear behaviors of reinforced concrete panels subjected to cyclic in-plane shear. *Trans AIJ, 403,* 105–117.

Orakcal, K., Ulugtekin, D., & Massone, L. M. (2012) Constitutive modeling of reinforced concrete panel behavior under cyclic loading. In *Proceedings, 15th World Conference on Earthquake Engineering*. Lisbon, Portugal.

Palermo, D., & Vecchio, F. J. (2003). Compression field modeling of reinforced concrete subjected to reversed loading: Formulation. *ACI Structural Journal, 100*(5), 616–625.

Pang, X. D., & Hsu, T. C. (1995). Behavior of reinforced concrete membrane elements in shear. *ACI Structural Journal, 92*(6), 665–679.

Pang, D., & Hsu, T. C. (1996). Fixed angle softened truss model for reinforced concrete. *ACI Structural Journal, 93*(2), 197–207.

Popovics, S. (1973). A numerical approach to the complete stress–strain curve of concrete. *Cement and Concrete Research, 3*(4), 583–599.

Saatcioglu, M., & Razvi, S. R. (1992). Strength and ductility of confined concrete. *ASCE Journal of Structural Engineering, 118,* 1590–1607.

Stevens, N. J. (1977). *Analytical modeling of reinforced concrete subjected to monotonic and reversed loadings* (Ph.D. thesis). Department of Civil Engineering, University of Toronto.

Stevens, N. J., Uzumeri, M., & Collins, M. P. (1991). Reinforced concrete subjected to reversed cyclic shear—Experiments and constitutive model. *ACI Structural Journal, 88*(2), 135–146.

Tassios, T. P., & Vintzēleou, E. N. (1987). Concrete-to-concrete friction. *ASCE Journal of Structural Engineering, 113*(4), 832–849.

Tripathi, M., Dhakal, R. P., Dashti, F., & Massone, L. M. (2018). Low-cycle fatigue behaviour of reinforcing bars including the effect of inelastic buckling. *Construction and Building Materials, 190,* 1226–1235.

Tsai, W. T. (1988). Uniaxial compressional stress–strain relation of concrete. *ASCE Journal of Structural Engineering, 114*(9), 2133–2136.

Vecchio, F. J. (1999). Towards cyclic load modeling of reinforced concrete. *ACI Structural Journal, 96*(2), 193–202.

Vecchio, F. J. (2000). Disturbed stress field model for reinforced concrete: formulation. *ASCE Journal of Structural Engineering, 126*(9), 1070–1077.

Vecchio, F. J., & Collins, M. P. (1986). The modified compression-field theory for reinforced concrete elements subjected to shear. *Journal of the American Concrete Institute, 83*(2), 219–231.

Vecchio, F. J., & Collins, M. P. (1993). Compression response of cracked reinforced concrete. *ASCE Journal of Structural Engineering, 119*(12), 3590–3610.

Publisher's Note